DESIGN OF CONTROL SYSTEMS FOR A QUADROTOR FLIGHT VEHICLE EQUIPPED WITH INERTIAL SENSORS

A MASTER'S THESIS

in

Mechatronics Engineering

Atılım University

by

ARDA ÖZGÜR KIVRAK

DECEMBER 2006

DESIGN OF CONTROL SYSTEMS FOR A QUADROTOR

FLIGHT VEHICLE EQUIPPED WITH INERTIAL SENSORS

A THESIS SUBMITTED TO

THE GRADUATE SCHOOL OF NATURAL AND APPLIED SCIENCES

OF

ATILIM UNIVERSITY

BY

ARDA ÖZGÜR KIVRAK

IN PARTIAL FULFILLMENT OF THE REQUIREMENTS FOR THE DEGREE OF

MASTER OF SCIENCE

IN

THE DEPARTMENT OF MECHATRONICS ENGINEERING

DECEMBER 2006

Approval of the Graduate School of (Name of the Graduate School)

_____

(Title and Name)

Director

I certify that this thesis satisfies all the requirements as a thesis for the degree of Master of Science/Arts.

_____

(Title and Name)

Head of Department

This is to certify that we have read this thesis and that in our opinion it is fully adequate, in scope and quality, as a thesis for the degree of Master of Science/Arts.

_____	_____
(Title and Name)	(Title and Name)
Co-Supervisor	Supervisor

Examining Committee Members

Asst.Prof.Dr.Bülent İRFANOĞLU	_____
Prof.Dr.Abdülkadir ERDEN	_____
Asst.Prof.Dr.Hakan TORA	_____
Asst.Prof.Dr.Serhat ERPOLAT	_____
Instr. Kutluk Bilge ARIKAN	_____

ABSTRACT

DESIGN OF CONTROL SYSTEMS FOR A QUADROTOR FLIGHT VEHICLE EQUIPPED WITH INERTIAL SENSORS

Kıvrak, Arda Özgür

M.S. Mechatronics Engineering Department

Supervisor: Kutluk Bilge Arıkan

December 2006 104 pages

This thesis reviews the Design of Control Systems for a Quadrotor Flight Vehicle Equipped with Inertial Sensors in detail. The control system is developed in Matlab/Simulink and real time implementation is achieved by using Simulink Real Time Windows Target utility. Linear Quadratic Regulator is designed for the stabilization of the attitude and shown to work in real time. The hardware consists of the data acquisition card, DC motor drivers, sensor set, the DC motors, and the DraganFlyer V Ti structure.

Keywords: Control, Quadrotor platform, Inertial Sensors, Matlab/Simulink, Real Time Windows Target (RTWT), Real Time Control, Linear Quadratic regulator.

ÖZ

ATALETSEL ALGILAYICILARA SAHİP DÖRT MOTORLU UÇUŞ ARACI İÇİN DENETİM SİSTEMLERİ TASARIMI

Kıvrak, Arda Özgür

Yüksek Lisans, Mekatronik Mühendisliği Bölümü

Tez Yöneticisi: Kutluk Bilge Arıkan

Aralık 2006, 104 sayfa

Bu calışma, dört motorlu uçuş aracının denetim sistemlerini incelemekte ve detayı ile vermektedir. Denetim sistemi Matlab/Simulink ortamında geliştirilmiş ve Simulink Real Time Windows Target kullanılarak gerçek zamanlı uygulaması yapılmıştır. Sistemin yönelim kararlılığının denetimi için Lineer Quadratik Regülatör tasarlanmış ve donanımlı sistemle gerçek zamanlı çalıştırılması gösterilmiştir. Donanım veri toplama kartı, doğru akım motor sürücü devresi, algılayıcı seti, doğru akım motorları ve DraganFlyer V Ti gövdesinden oluşmaktadır.

Anahtar Kelimeler: Denetim, Dört motorlu platform, Matlab/Simulink, Real Time Windows Target (RTWT), Gerçek zamanlı denetim, Lineer Quadratik Regülatör.

To My Parents

ACKNOWLEDGMENTS

I express sincere appreciation to my supervisor Kutluk Bilge Arıkan and Bülent Irfanoğlu for their guidance and insight throughout the research. And to my family, I offer sincere thanks for their continuous support and patience during this period.

TABLE OF CONTENTS

LIST OF TABLES

TABLE

LIST OF FIGURES

FIGURES

LIST OF ABBREVIATIONS

UAV – Unmanned Aerial Vehicle

MEMS – Micro Electromechanical Systems

INS – Inertial Navigation System

LQR – Linear Quadratic Regulator

EKF – Extended Kalman Filter

VTOL – Vertical Take Off and Landing

GPS – Global Positioning System

PHB – Popov, Hautus and Belevitch

PWM – Pulse Width Modulation

EADS – European Aeronautic Defense and Space Company

FEIT – Faculty of Engineering and Information Technology

ANU – Australian National University

STARMAC – Stanford Testbed of Autonomous Rotorcraft for Multi-Agent Control

A.M. – Amplitude Modulation

LIST OF SYMBOLS

p – pitch angular rate

q – roll angular rate

r – yaw angular rate

ϕ – pitch angle

θ – roll angle

ψ – yaw angle

x – position along x axis

y – position along y axis

z – position along z axis

u – linear speed along body x axis

v – linear speed along body y axis

w – linear speed along body z axis

I_x – The inertia around the x axis

I_y – The inertia around the y axis

I_z – The inertia around the z axis

CHAPTER 1

INTRODUCTION

Today, unmanned aerial vehicles (UAVs) are an important part of scientific study both in military and space studies. As a substitute for human piloted vehicles they are advantageous to protect human life in multiple dangerous environments. Their reliabilities in tough circumstances are much higher than their counter parts.

In this work the effort to produce quadrotor unmanned aerial vehicles (UAVs) at the Robotics Laboratory is presented. The main purpose of this study is to explore control methodologies for quadrotor unmanned aerial vehicles (UAVs).

Fixed-wing vehicles have long-range since they are energy efficient, but they lack the maneuverability required for many UAV tasks. For example, Blimps are easy to control when there are fewer disturbances like wind, and lift comes from natural buoyancy, but their maneuverability is limited. The helicopters have advantages over conventional fixed-wing aircraft and blimps on surveillance and inspection tasks, since they can take-off and land in limited space and can easily hover above targets. Moreover, helicopters have the advantage of maneuverability. Unfortunately, this advantage makes helicopters very hard to control, requiring sophisticated sensors and fast on-board computation [6].

The design of unmanned aerial vehicles involves the integration of various steps such as design, selection of sensors and developing controllers. These steps can not be treated separately. For example, one can not design a vehicle without considering the sensory input or the controllers that will be implemented, as these steps are closely related to each other [6].

In order to create an autonomous UAV, precise knowledge of the helicopter position and orientation is needed. This information can be obtained from Inertial Navigation

Systems (INS), Global Positioning Systems (GPS) or other sensors like sonar sensor. Typically, multiple sensors are used to overcome limitations of individual sensors, thereby increasing the reliability and decreasing the errors. Vision sensors are primarily used for estimating the relative positions of some target, like a landing site or a ground vehicle. Unfortunately the vision system is not as fast as a gyro, and it is not as reliable as other sensors due to sensitivity to changes in lighting conditions.

Our primary goal is to investigate the possibility of a real time working controller. Limited payload capacity may not permit the use of heavy navigation systems [6].

As a test bed a remote-controlled, model helicopter (Draganflyer V Ti) selected.

A Quadrotor is a four-rotor helicopter. It is an under-actuated, dynamic vehicle with four input forces and six degrees of freedom. Unlike regular helicopters that have variable pitch angle rotors, a quadrotor helicopter has four fixed-pitch angle rotors.

The basic motions of a Quadrotor are generated by varying the rotor speeds of all four rotors, thereby changing the lift forces. The helicopter tilts towards the direction of the slow spinning rotor, which enables acceleration along that direction. Therefore, control of the tilt angles and the motion of the helicopter are closely related and estimation of orientation (roll and pitch) is critical. Spinning directions of the rotors are set to balance the moments and eliminate the need for a tail rotor. This principle is also used to produce the desired yaw motions. A good controller should properly arrange the speed of each rotor so that only the desired states change.

1.1 Aim and Scope

In this study, it is desired to construct a nonlinear model of quadrotor in Simulink. It is aimed to design control algorithms that can stabilize the attitude based on the linearized model around hovering conditions and to implement the controller on physical platform using Simulink RTWT, PC and data acquisition card.

1.2 Layout of the Dissertation

Chapter 2 is the literature survey, which introduces some of the work that has been done on design, and control of flying vehicles. This chapter will also provide some background on sensors. Acceleration sensors, gyros and magnetometers are the sensors used in this work. Chapter 3 includes the derivations of the mathematical equations of the system. In Chapter 4 the LQR design for attitude stabilization is discussed. Chapter 5 explains the work about the structure and test bench. Real time controller implementation is discussed in chapter 6. Chapter 7 summarizes the tests and their results. And the final part chapter 8 is the conclusion of this study.

CHAPTER 2

LITERATURE SURVEY ABOUT QUAD-ROTOR SYSTEMS

2.1 Designs in Literature

In 1907, the Breguet Brothers constructed the first quad-rotor named Gyroplane No. 1 [1]. The flight was a good work to show the principle of a quadrotor. In 1922, Georges de Bothezat built a quadrotor with a rotor located at each end of a truss structure of intersecting beams, placed in the shape of a cross [1]. Experimental aircrafts X-19 and Bell X-22A are also designed as quad-tilt rotor aircrafts [1].

In time due to the tremendous improvements in manufacturing techniques and innovations in metallurgical material knowledge more precise and smaller sensors can now be produced. The Microelectromechanical Systems (MEMs) technology now allows the production of machine components such as gears with sizes in 10^{-6} meter range [15] [30]. Using this MEMS technology very small accelerometers, gyros and magnetometers are also produced [24] [25] [26] [27] [28], which caused the production of smaller strapdown inertial navigation systems. As a result of this improvement in technology very small quadrotors are developed around the world such as Mesicopter (Figure 1) [6] and Hoverbot [6]. There is also commercially available quadrotor named DraganFlyer (Figure 2)

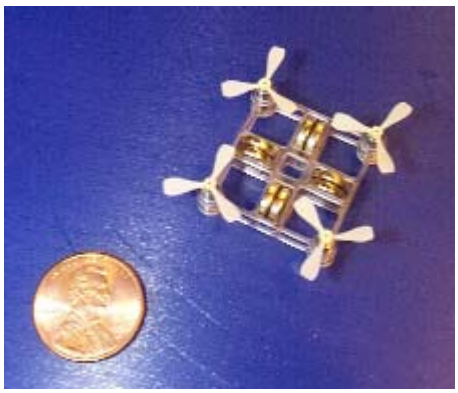

Figure 1 Mesicopter

Figure 2 DraganFlyer

Recently, there are several different studies in the literature about quadrotors. These works utilized different controllers, equipments and materials.

2.1.1 European Aeronautic Defense and Space Company

Quattrocopter (Figure 3) is a 65 cm electrically powered VTOL with a 20 min flight time. Its weight is 0.5 kg. Quattrocopter has flight range of 1 km. There are six inertial sensors in its six degree of freedom MEMS inertial measurement unit (IMU). In addition to six inertial sensors there is one GPS unit and air data sensors (gas sensors). Total measurement unit weighing 65 grams, consumes less than three watts at 5 V. The motors are detachable so that the system can be stored in a small space [43].

Figure 3 Quattrocopter

2.1.2 Pennsylvania State University

In Pennsylvania State university two different studies had been done on quadrotors [35] [6]. First is a master thesis (Figure 4) that had been done about a quadrotor test bench. The inertial measurement unit consists of three analog devices gyros (ADXRS150EB), one accelerometer (ADXL210EB). Attitude of the quadrotor is controlled with PI control law.

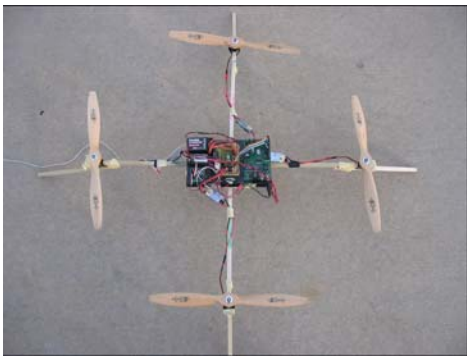

Figure 4 Quadrotor designed in Pennsylvania State University

Second work done in university of Pennsylvania (Figure 5) utilizes DraganFlyer as a testbed. It has external pan-tilt ground and on-board cameras in addition to the three onboard gyroscopes. One camera placed on the ground captures the motion of five 2.5 cm colored markers present underneath the DraganFlyer, to obtain pitch, roll and yaw angles and the position of the quadrotor by utilizing a tracking algorithm and a conversion routine. In other words, two-camera method has been introduced for estimating the full six degrees of freedom (DOF) pose of the helicopter. Algorithm routines ran in an off board computer. Due to the weight limitations GPS or other accelerometers could not be add on the system. The controller obtained the relative positions and velocities from the cameras only.

Two methods of control are studied – one using a series of mode-based, feedback linearizing controllers and the other using a back-stepping control law. The helicopter was restricted with a tether to vertical, yaw motions and limited x and y translations. Simulations performed on MATLAB-Simulink show the ability of the controller to perform output tracking control even when there are errors on state estimates.

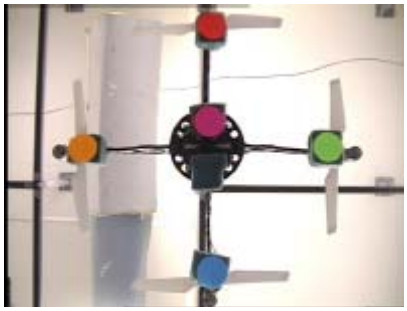

Figure 5 Quadrotor tracking with a camera

2.1.3 Middle East Technical University

Three orthogonal piezoelectric gyro used in the system designed in Middle East Technical University (Figure 6) to control the attitude of the quadrotor [32]. The attitude controlled with a Linear Quadratic Regulator and PD controller. Frame consists of 45 cm rectangular aluminum profiles.

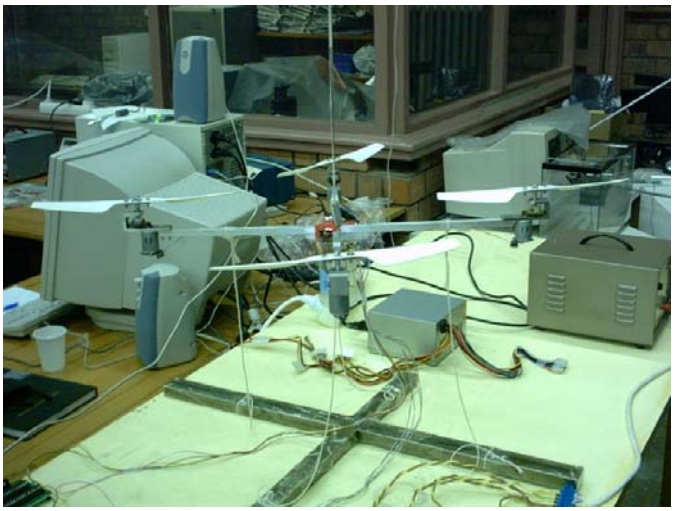

Figure 6 Quadrotor designed in Middle East Technical University, Turkey

2.1.4 Australian National University

The X4-Flyer developed in ANU [14] consists of a HC-12 a single board computer, developed at QCAT that was used as the signal conditioning system. This card uses two HC-12 processors and outputs PWM signals that control the speed drivers directly, inputs PWM signals from an R700 JR Slimline RC receiver allowing direct plot input from a JP 3810 radio transmitter and has two separate RS232 serial channels, the first used to interface with the inertial measurement unit (IMU) and second used as an asynchronous data linked to the ground based computer.

As an IMU the most suitable unit considered was the EiMU embedded inertial measurement unit developed by the robotics group in QCAT, CSIRO weighs 50-100g. Crossbow DMU-6 is also used in the prototype. It weighs 475g.

The rotor used is an 11'' diameter APC-C2 2.9:1 gear system included 6'' per revolution pitch with a maximum trust of 700grams. An the motors are Johnson 683 500 series motors

The speed controller used is MSC30 B with a weight 26g rated 30A at 12V

The pilot augmentation control system is used. A double lead compensator is used for the inner loop. The final setup is shown in Figure 7.

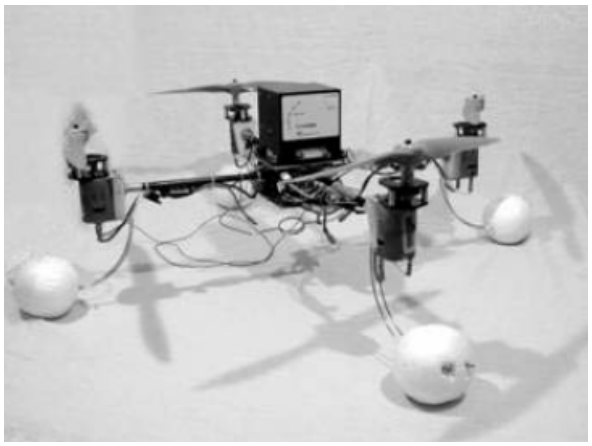

Figure 7 The X4-Flyer developed in FEIT, ANU

2.1.5 University of British Columbia Vancouver, BC, Canada

Setup developed in Department of Electrical and Computer Engineering University of British Columbia Vancouver, BC, Canada [4]. This work focused on the nonlinear modelling of a quad rotor UAV. An experimental system including a flying mill, a DSP system, a programmed microprocessor and a wireless transmitter have been used to test the flight controller. Based on the nonlinear model, an $H\infty$ loop shaping controller is designed for stabilization, speed, throttle and yaw control.

A microprocessor, PIC16F877, is programmed to transfer the control data to a pulse width modulated signal in order to reduce significant CPU load which otherwise

would have been associated with the DS1102. This signal is further used to control the four rotors of the Draganflyer III via a 4 channel Futaba radio transmitter working in training mode.

In order to carry out flight control experiments, an experimental rig including a custom designed flying mill, a personal computer, dSPACE DSP board, a microprocessor pulse modulator, a radio transmitter and the Draganflyer III was built. A picture of the flying mill is shown in Figure 8. The steel base and carbon fiber boom limit the flight route of the UAV Draganflyer III to a half sphericity of 1 meter radius.

Based on the nonlinear model, an $H\infty$ loop shaping controller is designed for stabilization, speed, throttle and yaw control. A constraint model based predictive control (MBPC) controller is implemented for longitudinal and lateral trajectory control.

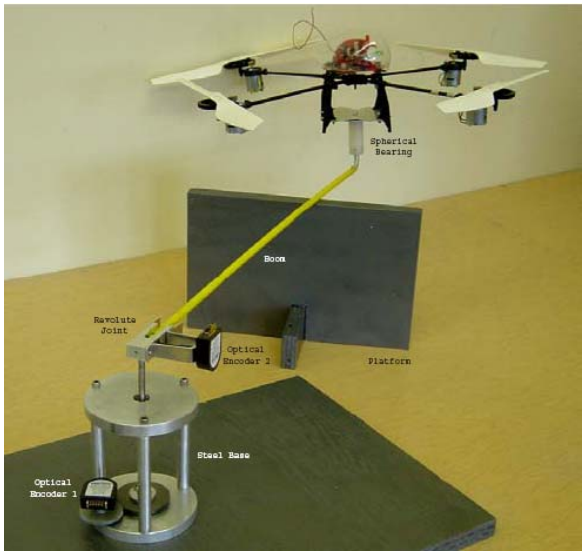

Figure 8 Setup developed in Department of Electrical and Computer Engineering University of British Columbia Vancouver, BC, Canada

2.1.6 Cornell University

The Autonomous Flying Vehicle (AFV) project at Cornell University [10] has been an ongoing attempt to produce a reliable autonomous hovering vehicle.

In the thrust system MaxCim motors were used. The final vehicle weighed approximately 6.22 kg.

Initially an Extended Kalman Filter was designed to handle the estimation of both the state and the six IMU sensor bias parameters. This filter found to be cumbersome to implement, due to extremely large and complex Jacobian terms and instead a square root implementation of a Sigma Point Filter (SRSPF) was considered. The final picture of the quadrotor is shown in Figure 9.

Figure 9 Quadrotor designed in Cornell University

2.1.7 Swiss Federal Institute of Technology

In the study done at Swiss Federal Institude of Technology [13] the mechanical design, dynamic modelling, sensing, and control of an indoor VTOL autonomous robot OS43 is presented. The 3 DOF are locked.

From a PC and through a standard RS232 port, orders were sent to the test bench. The RS232 to I2C module translates the serial signals to the I2C bus motor modules. These modules integers a P.I.D regulator on a PIC16F876 microcontroller and are capable of open or closed loop operation in position, speed or torque control. The MT9-B8 IMU9 estimates with a Kalman filter the 3D orientation data and give the calibrated data of acceleration and angular velocity. It weights about 33g and communicates at 115kbps. The captured motion from the 3D universal joint decoded to extract absolute orientation information, by the help of the micro optical encoders in each axis.

The cross is made with carbon rods thus vehicle, the mass of which is around 240 grams, is lightweight.The OS4 test bench has four propulsion group, each composed of a 29g motor including magnetic encoders, a 6g-gear box and a 6g propeller.

Before implementation on the real system, several simulations had been performed on Matlab. The controller's task was to stabilize the height while compensating the initial error on the roll, pitch and yaw angles. The real system suffered from undesired but unavoidable delays and actuator saturation. The delays were reported to be mainly due to RS232 communications and the actuator time constant. To emulate these lacks, two Simulink discrete-step delay blocks had been introduced in the feedback loop and on the actuators. Saturation level depends on the chosen actuators. The experimental setup for this study is shown in the Figure 10.

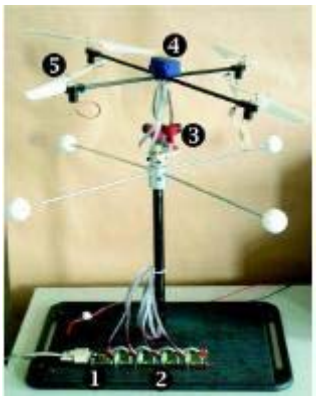

Figure 10 Quadrotor designed in Swiss Federal Institude of Technology

2.1.8 University of Technology in Compiegne, France

Quadrotor system, manufactured by the Draganfly Innovations Inc., was used as the test base [8]. The four control signals were transmitted by a Futaba Skysport 4 radio.

The radio and the PC (INTEL Pentium 3) were connected using data acquisition cards (ADVANTECH PCL-818HG and PCL-726). The connection in the radio is directly made to the joystick potentiometers for the collective, yaw, pitch and roll controls. In order to simplify the tuning of the controller and for flight security reasons, several switches were introduced in the PC-radio interface so that each control input can operate either in manual mode or in automatic control. Therefore the control inputs that are handled manually were selected by the pilot while the other control inputs are provided by the computer.

The Polhemus was connected via RS232 to the PC. This type of sensor was reported to be very sensitive to electromagnetic noise and it was install as far as possible from the electric motors and their drivers. The Draganfly III has three onboard gyros that helped the mini-rotorcraft's stabilization. The dynamic model of the four rotor rotorcraft was obtained via a Lagrange approach. And the proposed controller was based on Lyapunov analysis using a nested saturation algorithm. The picture of the setup when it was hovering is shown in Figure 11.

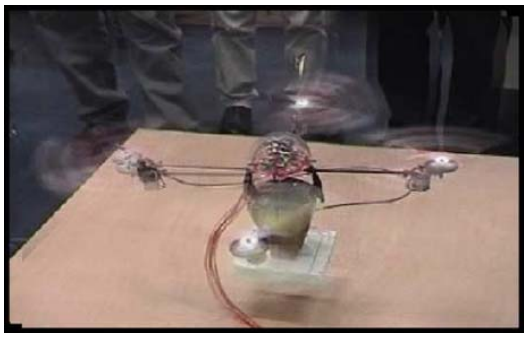

Figure 11 Quadrotor designed in University of Technology in Compiegne, France

2.1.9 Stanford University

The name of the project that is worked on in stanford university is called STARMAC [45]. STARMAC consists of four X4-flyer rotorcraft that can autonomously track a given waypoint trajectory. This trajectory generated by novel trajectory planning algorithms for multi agent systems. STARMAC project aims a system fully capable of reliable autonomous waypoint tracking, making it a useful testbed for higher level algorithms addressing multiple-vehicle coordination.

The base system is the off-the-shelf four-rotor helicopter called the DraganFlyer III, which can lift approximately 113,40 grams of payload and fly for about ten minutes at full throttle. The open-loop system is unstable and has a natural frequency of 60 Hz, making it almost impossible for humans to fly. An existing onboard controller slows down the system dynamics to about 5 Hz and adds damping, making it pilotable by humans. It tracks commands for the three angular rates and thrust. An upgrade to Lithium-polymer batteries has increased both payload and flight duration, and has greatly enchanced the abilities of the system.

For attitude measurement, an off-the-shelf 3-D motion sensor developed by Microstrain, the 3DM-G was used. This all in one IMU provides gyro stabilized attitude state information at a remarkable 50 Hz. For position and velocity measurement, Trimble Lassen LP GPS receiver was used. To improve altitude information a downward-pointing sonic ranger (Sodar) by Acroname were used, especially for critical tasks such as take off and landing. The Sodar has a sampling rate of 10 Hz, a range of 6 feet, and an accuracy of a few centimeters, while the GPS computes positions at 1 Hz, and has a differential accuracy of about 0.5 m in the horizontal direction and 1 m in the vertical. To obtain such accuracies, DGPS planned be implemented by setting up a ground station that both receives GPS signals and broadcasts differential correction information to the flyers.

All of the onboard sensing is coordinated through two Microchip 40 MHz PIC microcontrollers programmed in C. Attitude stabilization were performed on board at 50 Hz, and any information was relayed upon request to a central base station on the ground. Communication is via a Bluetooth Class II device that has a range of over

150 ft. The device operates in the 2.4 GHz frequency range, and incorporates band-hopping, error correction and automatic retransmission. It is designed as a serial cable replacement and therefore operates at a maximum bandwidth of 115.2 kbps. The communication scheme incorporates polling and sequential transmissions, so that all flyers and the ground station simultaneously operate on the same communication link. Therefore, the bandwidth of 115.2 kbps is divided among all flyers.

The base station on the ground performs differential GPS and waypoint tracking tasks for all four flyers, and sends commanded attitude values to the flyers for position control. Manual flight is performed via standard joystick input to the ground station laptop. Waypoint control of the flyers was performed using Labview on the groundstation due to its ease of use and on the fly modification ability. Control loops have been implemented using simple PD controllers. The system while hovering is shown in Figure 12.

Figure 12 Quadrotor designed in Stanford University

2.1.10 Australian National University, Canberra, Australia

Current work on the X-4 Flyer aims to solve two problems: thrust and stability. X4 Flyer has weight of 2 kg with a length of 70 cm an 11 inch diameter rotors.

The electronics are substantially the same as the Mark I, although a lighter sensor unit has replaced the original Crossbow IMU. The control board and ‘Eimu’ IMU were built by the CSIRO ICT Centre. The control board is a dual HC-12 microprocessor card with digital I/O. The Eimu is a full six-axis IMU with magnetometer. It is operated in vertical gyro mode to obtain inertial frame reference

angles. There is room inside the frame for mounting the Eimu as close to the centre of gravity as possible.

Unlike the Mark I, the Mark II incorporates simple onboard proportional-integral-derivative control. The previous iteration used a slow, off-board control system connected to the flyer by a tether. It is anticipated that the convenient aerodynamics of the X-4 had made sophisticated control unnecessary. In conjunction with onboard power, this allowed the flyer to be entirely self-contained. MARK II shown in figure 13.

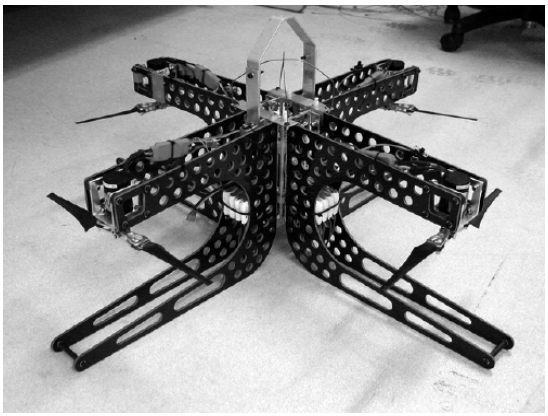

Figure 13 X-4 Flyer Mark II.

2.2 Applied Control Systems

For the control of UAVS there are several methodologies used in the literature. Control systems that are used for the control of a helicopter type flying machine are: robust feedback controllers based on H_∞ techniques [4], fuzzy control, PD controllers [3], back-stepping controllers [3], Neural-Network Adaptive Flight Control [3]. For the experimentation done on the Stanford draganflyer UAVS, nonlinear control methods are used that uses discrete-time dynamic inversion, under input saturation [7]. Another study done at the University of Pennsylvania showed another control example, which used a vision based control methodology for the control of UAVS [6].

2.3 Employed Sensors

In order to establish a certain control mechanism for a system the changing states and properties of its internal and external environment must be known to the system. In other words the important parameters for the system control must be monitored and fed back to the system.

In order to establish this requirement some sensors must be used that are specific for different observation environments. For instance, for the control of the navigation of a flying machine an Inertial Measurement Unit is needed. This unit is composed of some several types of sensors such as accelerometers, gyros, etc. Gyro type sensors are used in order to sense the rate of change of the rotation around a certain axis where as accelerometer type sensors are used for the detection of the linear acceleration of the system. There are several types of gyros and accelerometers on the market. MEMS accelerometers for instance work on the principle of capacitive changes where as piezo-accelerometers uses piezoelectricity principle. The same is true for the gyros also. Fiber optic gyros are expensive and bulky whereas MEMS gyros are cheap and light.

In order to detect the number of revolutions of a rotating shaft in the system, an encoder or a magnetic rotation sensor can be used. This rotating shaft for example can be the shaft of a propeller of a helicopter. Determination of the rotation speed of this propeller shaft is a vital job for the control of the helicopter body.

For the determination of the position of the flying machine on 3D space a differential GPS sensing is required. This system when used in cooperation with inertial navigation system navigation becomes less erroneous and much more reliable. In addition to those sensor sets some compass and Magnetometer type sensors are also used in some systems to detect the earth's magnetic field for the calculation of the direction and altitude parameters. As a proximity sensor Sonar and Radar Altimeters are used [7]. They give information about the proximity obstacle and target positions. In order to monitor the system sources like batteries, and fuel condition Vehicle Telemetry sensors are used [10]

CHAPTER 3

MATHEMATICAL MODEL OF THE HOVERING PLATFORM

3.1 Assumptions of the Model

The physical setup is a complex structure and without simplifying assumptions it is cumbersome to derive the mathematical model of it. The following are some assumptions that are used in developing the mathematical model of the quadrotor.

- The carbon fiber structure is supposed to be rigid.
- The helicopter has a perfectly symmetrical structure so; the matrix of inertia will supposed to be diagonal.
- The bearing pressure and the trail of each engine are proportional to the square speed, which is an approximation very close to the aerodynamic behavior.
- hovering condition is assumed.

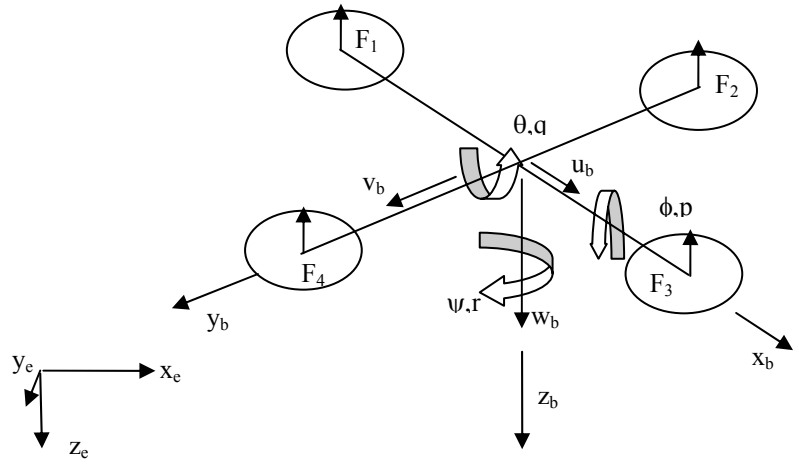

Figure 14 All of the States (b stands for body and e stands for earth)

3.2 Derivation of the State Equations

The quadrotor system is a six degrees of freedom system defined with twelve states. Six out of twelve states govern the attitude of the system (Figure 14). These include the angles (ϕ, θ, ψ) and angular rates (p, q, r) around the three orthogonal body axes. The other six states are the three positions and three linear velocities of the center of mass of the quadrotor with respect to a fixed reference frame (earth fixed frame). Note that there are two coordinate frames one of them is fixed at the ground and the other is fixed at the center of gravity of the quadrotor. In order to derive the state equations with respect to those frames the rotation matrices between two coordinate frames must be derived.

For each axis transformation matrices can be written as,

$$R_x = \begin{bmatrix} 1 & 0 & 0 \\ 0 & \cos\phi & -\sin\phi \\ 0 & \sin\phi & \cos\phi \end{bmatrix} \tag{1}$$

$$R_y = \begin{bmatrix} \cos\theta & 0 & \sin\theta \\ 0 & 1 & 0 \\ -\sin\theta & 0 & \cos\theta \end{bmatrix} \tag{2}$$

$$R_z = \begin{bmatrix} \cos\psi & -\sin\psi & 0 \\ \sin\psi & \cos\psi & 0 \\ 0 & 0 & 1 \end{bmatrix} \tag{3}$$

Resultant transformation matrix

$$R = R_z.R_y.R_x \tag{4}$$

$$R_y.R_x = \begin{bmatrix} \cos\theta & \sin\theta.\sin\phi & \sin\theta.\cos\phi \\ 0 & \cos\phi & -\sin\phi \\ -\sin\theta & \sin\phi.\cos\theta & \cos\theta.\cos\phi \end{bmatrix} \tag{5}$$

$$R = R_z.R_y.R_x = \begin{bmatrix} \cos\psi & -\sin\psi & 0 \\ \sin\psi & \cos\psi & 0 \\ 0 & 0 & 1 \end{bmatrix} . \begin{bmatrix} \cos\theta & \sin\theta.\sin\phi & \sin\theta.\cos\phi \\ 0 & \cos\phi & -\sin\phi \\ -\sin\theta & \sin\phi.\cos\theta & \cos\theta.\cos\phi \end{bmatrix} \tag{6}$$

$$R = \begin{bmatrix} \cos\psi.\cos\theta & \cos\psi.\sin\theta.\sin\phi - \cos\phi.\sin\psi & \cos\psi.\sin\theta.\cos\phi + \sin\psi.\sin\phi \\ \sin\psi.\cos\theta & \sin\psi.\sin\theta.\sin\phi + \cos\psi.\cos\phi & \sin\psi.\sin\theta.\cos\phi - \sin\phi.\cos\psi \\ -\sin\theta & \sin\phi.\cos\theta & \cos\theta.\cos\phi \end{bmatrix} \quad (7)$$

Linear velocities along body axes can be transformed into inertial frame using the transformation matrix R given above

$$\dot{x} = \frac{d}{dt}\begin{bmatrix} x_E & y_E & z_E \end{bmatrix}^T = R\begin{bmatrix} u & v & w \end{bmatrix}^T \quad (8)$$

$$\begin{bmatrix} \dot{x} \\ \dot{y} \\ \dot{z} \end{bmatrix} = R.\begin{bmatrix} u \\ v \\ w \end{bmatrix} \quad (9)$$

$$\dot{x} = a + b + c \quad (10)$$

where,

$a = \cos\psi.\cos\theta.u$

$b = (\cos\psi.\sin\theta.\sin\phi - \cos\phi.\sin\psi).v$

$c = (\cos\psi.\sin\theta.\cos\phi + \sin\psi.\sin\phi).w$

$$\dot{y} = d + e + f \quad (11)$$

where,

$d = \sin\psi.\cos\theta.u$

$e = (\sin\psi.\sin\theta.\sin\phi + \cos\psi.\cos\phi).v$

$f = (\sin\psi.\sin\theta.\cos\phi - \sin\phi.\cos\psi)w$

$$\dot{z} = -\sin\theta.u + \sin\phi.\cos\theta.v + \cos\theta.\cos\phi.w \quad (12)$$

Angular rates along body axes can be transformed into Euler rates using the transformation matrix T given below

$$\frac{d}{dt}\begin{bmatrix} \phi & \theta & \psi \end{bmatrix}^T = T\begin{bmatrix} p & q & r \end{bmatrix}^T \quad (13)$$

$$T = \begin{bmatrix} 1 & \tan\theta.\sin\phi & \tan\theta.\cos\phi \\ 0 & \cos\phi & -\sin\phi \\ 0 & \sec\theta.\sin\phi & \sec\theta.\cos\phi \end{bmatrix} \tag{14}$$

$$\begin{bmatrix} \dot{\phi} \\ \dot{\theta} \\ \dot{\psi} \end{bmatrix} = T. \begin{bmatrix} p \\ q \\ r \end{bmatrix} \tag{15}$$

$$\dot{\phi} = p + q.\tan\theta.\sin\phi + r.\tan\theta.\cos\phi \tag{16}$$

$$\dot{\theta} = q.\cos\phi - r.\sin\phi \tag{17}$$

$$\dot{\psi} = q.\sec\theta.\sin\phi + r.\sec\theta.\cos\phi \tag{18}$$

For the system at hand the "Newton's Second Law of Motion" can be written as

$$F=ma \tag{19}$$

where m is the mass of the system, a is the acceleration and F is the net force acting on the body, then,

$$(F+G)\frac{1}{m} = \frac{d}{dt}V = \begin{bmatrix} \dot{u} & \dot{v} & \dot{w} \end{bmatrix}^T + \begin{bmatrix} p & q & r \end{bmatrix}^T \times \begin{bmatrix} u & v & w \end{bmatrix}^T \tag{20}$$

Here G is denoting the gravitational force acting on the body. If the body acceleration term is taken out,

$$\begin{bmatrix} \dot{u} & \dot{v} & \dot{w} \end{bmatrix}^T = \frac{1}{m}\begin{bmatrix} F_x & F_y & F_z \end{bmatrix}^T + R^T \begin{bmatrix} 0 & 0 & g \end{bmatrix}^T - \begin{bmatrix} p & q & r \end{bmatrix}^T \times \begin{bmatrix} u & v & w \end{bmatrix}^T \tag{21}$$

The cross product term can be opened as,

$$\begin{bmatrix} p & q & r \end{bmatrix}^T \times \begin{bmatrix} u & v & w \end{bmatrix}^T = \begin{bmatrix} q.w - r.v \\ r.u - p.w \\ p.v - q.u \end{bmatrix} \tag{22}$$

And also the gravitational acceleration vector can be rotated as,

$$R^T \begin{bmatrix} 0 & 0 & g \end{bmatrix}^T = \begin{bmatrix} \cos\psi.\sin\theta.\cos\phi.g + \sin\psi.\sin\phi.g \\ \sin\psi.\sin\theta.\cos\phi.g - \sin\phi.\cos\psi.g \\ \cos\theta.\cos\phi.g \end{bmatrix} \tag{23}$$

Then the rate of the body linear velocities can be calculated as,

$$\begin{bmatrix} \dot{u} \\ \dot{v} \\ \dot{w} \end{bmatrix} = \frac{1}{m}\begin{bmatrix} F_x \\ F_y \\ F_z \end{bmatrix} + \begin{bmatrix} \cos\psi.\sin\theta.\cos\phi.g + \sin\psi.\sin\phi.g \\ \sin\psi.\sin\theta.\cos\phi.g - \sin\phi.\cos\psi.g \\ \cos\theta.\cos\phi.g \end{bmatrix} - \begin{bmatrix} q.w - r.v \\ r.u - p.w \\ p.v - q.u \end{bmatrix} \tag{24}$$

$$\dot{u} = \frac{1}{m}.F_x + g.\cos\psi.\sin\theta.\cos\phi + g.\sin\psi.\sin\phi - q.w + r.v \tag{25}$$

$$\dot{v} = \frac{1}{m}.F_y + g.\sin\psi.\sin\theta.\cos\phi - g.\sin\phi.\cos\psi - r.u + p.w \tag{26}$$

$$\dot{w} = \frac{1}{m}.F_z + g.\cos\theta.\cos\phi - p.v + q.u \tag{27}$$

By equating the change of angular momentum to the net moment on the system,

$$\frac{dH}{dt} = \frac{d}{dt}I.[p\ q\ r]^T = I.[\dot{p}\ \dot{q}\ \dot{r}]^T + [p \quad q \quad r]^T \times I.[p \quad q \quad r]^T \tag{28}$$

$$[M_x\ M_y\ M_z]^T = I.[\dot{p}\ \dot{q}\ \dot{r}]^T + [p \quad q \quad r]^T \times I.[p \quad q \quad r]^T \tag{29}$$

$$[\dot{p}\ \dot{q}\ \dot{r}]^T = I^{-1}.[M_x\ M_y\ M_z]^T - I^{-1}.[p \quad q \quad r]^T \times I.[p \quad q \quad r]^T \tag{30}$$

So 12 state equations can be written as,

$$\dot{x} = a + b + c \tag{31}$$

where,

$a = \cos\psi.\cos\theta.u$
$b = (\cos\psi.\sin\theta.\sin\phi - \cos\phi.\sin\psi).v$
$c = (\cos\psi.\sin\theta.\cos\phi + \sin\psi.\sin\phi).w$

$$\dot{y} = d + e + f \tag{32}$$

where,

$$d = \sin\psi.\cos\theta.u$$

$$e = (\sin\psi.\sin\theta.\sin\phi - \cos\psi.\cos\phi).v$$

$$f = (\sin\psi.\sin\theta.\cos\phi - \sin\phi.\cos\psi)w$$

$$\dot{z} = -\sin\theta.u + \sin\phi.\cos\theta.v + \cos\theta.\cos\phi.w \tag{33}$$

$$\dot{\phi} = p + q.\tan\theta.\sin\phi + r.\tan\theta.\cos\phi \tag{34}$$

$$\dot{\theta} = q.\cos\phi - r.\sin\phi \tag{35}$$

$$\dot{\psi} = q.\sec\theta.\sin\phi + r.\sec\theta.\cos\phi \tag{36}$$

$$\dot{u} = \frac{1}{m}.F_x + g.\cos\psi.\sin\theta.\cos\phi + g.\sin\psi.\sin\phi - q.w + r.v \tag{37}$$

$$\dot{v} = \frac{1}{m}.F_y + g.\sin\psi.\sin\theta.\cos\phi - g.\sin\phi.\cos\psi - r.u + p.w \tag{38}$$

$$\dot{w} = \frac{1}{m}.F_z + g.\cos\theta.\cos\phi - p.v + q.u \tag{39}$$

$$\begin{bmatrix}\dot{p} & \dot{q} & \dot{r}\end{bmatrix}^T = I^{-1}.\begin{bmatrix}M_x & M_y & M_z\end{bmatrix}^T - I^{-1}.\begin{bmatrix}p & q & r\end{bmatrix}^T \times I.\begin{bmatrix}p & q & r\end{bmatrix}^T \tag{40}$$

State Vector defining the attitude dynamics is given below

$$x = \begin{bmatrix}p & q & r & \phi & \theta & \psi\end{bmatrix}^T \tag{41}$$

3.3 Motor-Propeller Models

In the above equations the forces acting onto the body along x, y and z directions are required. Since our aim is an indoor flight the disturbances are assumed to be negligible. Therefore the main forces acting on the body are the propeller thrusts, motor torques and the gravitational forces. Rather than deriving a cumbersome dynamic model, a linear model is derived for the motors. In order to find a linear experimental relationship between the motor voltage and propeller thrusts, a test setup has been prepared, (Figure 15).

Figure 15 Motor test setup for thrust calculation.

In this setup the motor is constrained in a thick metal to keep it in a certain orientation. And this module is placed on the digital 1% precise scale. Then the motor voltage and current measured at 0.1 V increments. The results of this experiment are shown in the graphs below (Figure 16, Figure 17, Figure 18, Figure 19).

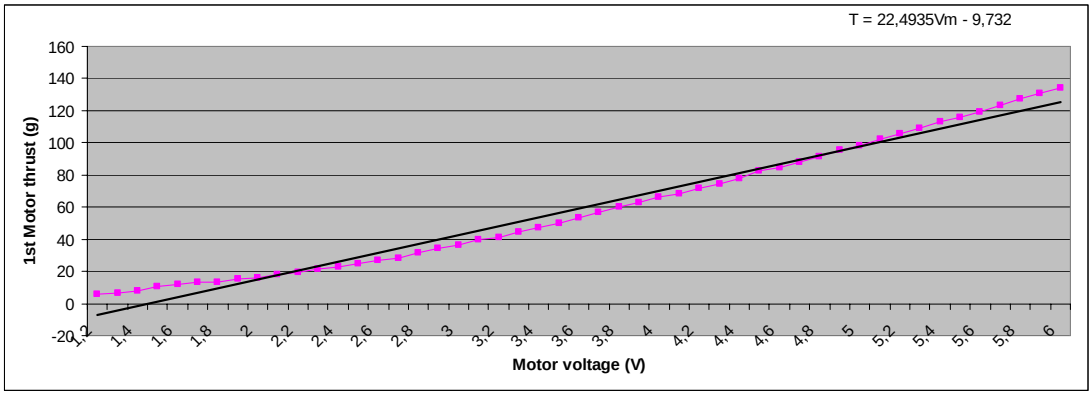

Figure 16 Test results of the 1st Motor (voltage vs. thrust(T))

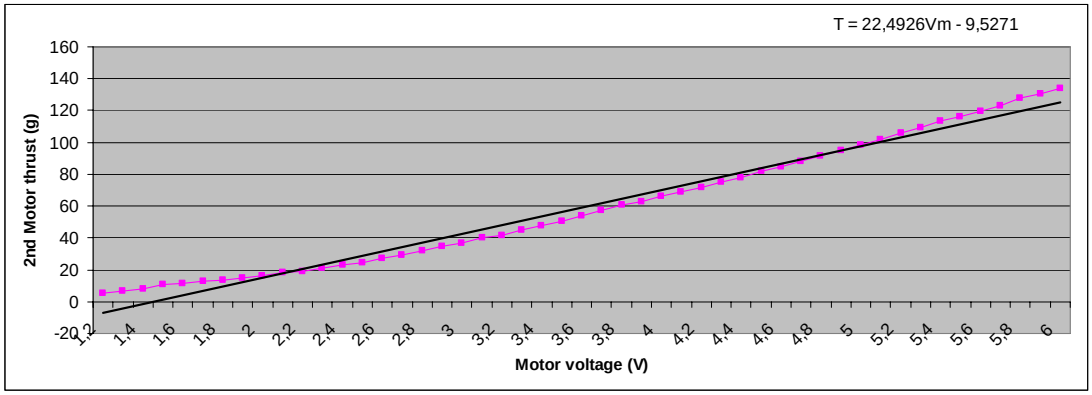

Figure 17 Test results of the 2nd motor (voltage vs. thrust(T))

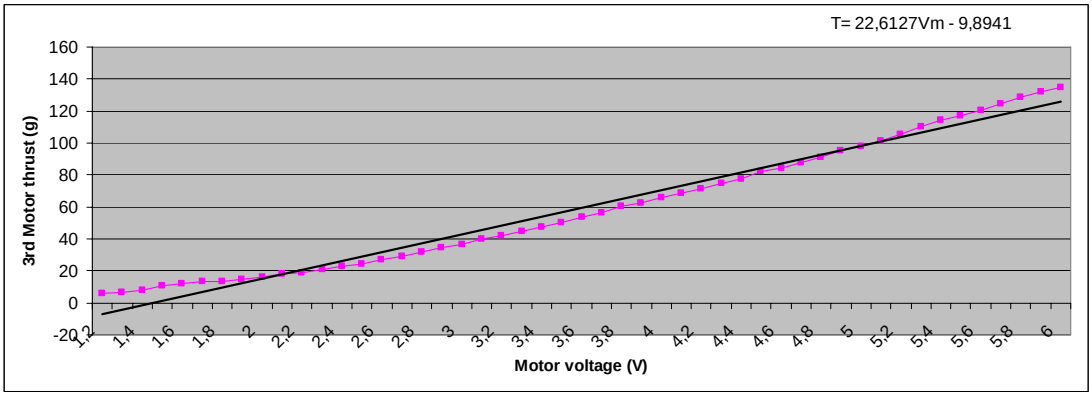

Figure 18 Test results of the 3rd motor (voltage vs. thrust(T))

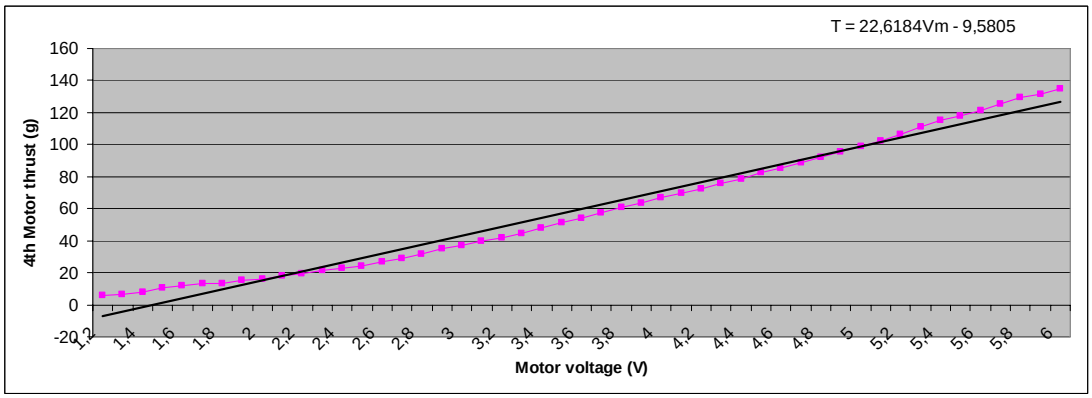

Figure 19 Test results of the 4th motor (voltage vs. thrust(T))

It is seen in the experiments that this relationship between the motor thrust and its voltage is a nonlinear one. In order to use LQR, this motor relation must be linearized. For this purpose a best fitting line to the nonlinear curve is derived using least squares method and it is this line that is used in the model.

For each motor the line representing their behavior is derived, which are given as;

$$F1=9.81*(22.4935*V_{m1}-9.732)/1000 \quad (42)$$

$$F2=9.81*(22.4926*V_{m2}-9.5271)/1000 \quad (43)$$

$$F3=9.81*(22.6127*V_{m3}-9.8941)/1000 \quad (44)$$

$$F4=9.81*(22.6184*V_{m4}-9.5805)/1000 \quad (45)$$

Here F's are the motor thrust values in Newtons. And V_m's, which are the inputs of the system, are the motor voltages in volts. Therefore, total thrust of the motors can be calculated as;

$$Fz=-(F1+F2+F3+F4) \quad (46)$$

And the moment forces can be approximated as;

$$Mx=L*(F2-F4) \quad (47)$$

$$My=L*(F1-F3) \quad (48)$$

$$Mz=-c*F1+c*F2-c*F3+c*F4 \quad (49)$$

Here L is equal to the distance from the free end of the frame bars to the center of gravity of the quadrotor which is equal to 0.21 m for the quadrotor system at hand. And c is a constant relating the trust forces to the moment around the vertical body axis, the value of which is taken as 0.1 from a similar study done in literature [32].

The disturbances along x and y body axis are assumed to be negligible in an indoor flight condition so the forces acting along those axes are taken to be zero i.e.

$$Fx=0 \quad (50)$$

$$Fy=0 \quad (51)$$

In derivation of the mathematical model the inertial parameters of the system are needed. The masses of different parts of the system are given below as well as the inertias about the three orthogonal axes. Moment of inertias are taken from a similar study done in literature [6] so they are approximations rather than being exact.

Table 1 Inertial Parameters

PARTS	MASS (Grams)
1 BLADE	9
1 MOTOR	51
CARBON STICKS	3.46
FULL DRAGANFLYER	467.21
1 MOTOR HOLDER	2.82
BATTERY	91.13
HARDWARE	48.80
PLASTIC CAP	9.00
FINAL TOTAL MASS	320
AXIS	INERTIAS ($kg.m^2$)
$I_{x\,(body)}$	0.0142
$I_{y\,(body)}$	0.0142
$I_{z\,(body)}$	0.0071

3.4 Linearization of the Nonlinear State Equations

The governing state equations are non-linear. These equations have to be linearized about the stable hovering conditions. Linearizations of the nonlinear state equations are done by using jacobians of the nonlinear state equations with respect to the states and the inputs around hovering conditions $x_0 = \begin{bmatrix} 0 & 0 & 0 & 0 & 0 & 0.1 \end{bmatrix}$.

Given a set of state equations $y = f(x)$ in n equations in n state variables $x_1,..,x_n$, the Jacobian matrix of a set of state equations can be calculated as shown in equation 52.

$$\frac{\partial f}{\partial x} = \begin{bmatrix} \frac{\partial f_1}{\partial x_1} & \frac{\partial f_1}{\partial x_2} & \cdots \\ \frac{\partial f_2}{\partial x_1} & \frac{\partial f_2}{\partial x_2} & \cdots \\ \vdots & \vdots & \ddots \\ & & \end{bmatrix} \tag{52}$$

The Jacobian matrix of the non-linear state equations with respect to the states at the given initial conditions is given in the equation 53.

$$A = \frac{\partial f}{\partial x} = \begin{bmatrix} 0 & 0 & 0 & 0 & 0 & 0 \\ 0 & 0 & 0 & 0 & 0 & 0 \\ 0 & 0 & 0 & 0 & 0 & 0 \\ 1 & 0 & 0 & 0 & 0 & 0 \\ 0 & 0.995 & -0.0998 & 0 & 0 & 0 \\ 0 & 0.0998 & 0.995 & 0 & 0 & 0 \end{bmatrix}_{x=x_0} \tag{53}$$

The input matrix, B, of the state-space representation is formed by taking the jacobian of the state equations with respect to the input vector, u (equation 54). The inputs of the system are the motor voltages which are denoted with letters $u_1,..,u_4$.

$$u(t)=\begin{bmatrix} u_1 \\ u_2 \\ u_3 \\ u_4 \end{bmatrix} \tag{54}$$

The matrix B for the states at hovering condition is shown in equation 55.

$$B=\frac{\partial f}{\partial u}=\begin{bmatrix} 0 & 14.1622 & 0 & -14.1622 \\ 14.1622 & 0 & -14.1622 & 0 \\ -18.6049 & 18.6049 & -18.6049 & 18.6049 \\ 0 & 0 & 0 & 0 \\ 0 & 0 & 0 & 0 \\ 0 & 0 & 0 & 0 \end{bmatrix}_{x=x_0} \tag{55}$$

Three gyroscopes measure the set of angular velocity components $\{p,q,r\}$, one two axis accelerometer is assumed to measure pitch (ϕ) and roll (θ) angles, and one magnetometer measures the yaw angle (ψ), which are all state variables. The direct transition matrix D is taken to be zero because there is no direct coupling between input and output of the system. On the other hand, the output matrix C given in equation (56) consists of the measurement of three six state variables by the sensors.

$$C=\begin{bmatrix} 1 & 0 & 0 & 0 & 0 & 0 \\ 0 & 1 & 0 & 0 & 0 & 0 \\ 0 & 0 & 1 & 0 & 0 & 0 \\ 0 & 0 & 0 & 1 & 0 & 0 \\ 0 & 0 & 0 & 0 & 1 & 0 \\ 0 & 0 & 0 & 0 & 0 & 1 \end{bmatrix} \tag{56}$$

The output of the system turns out to be as;

$$y = Cx + Du = \begin{bmatrix} p \\ q \\ r \\ \phi \\ \theta \\ \psi \end{bmatrix} \tag{57}$$

Where,

p – the pitch angular rate,
q – the roll angular rate,
r – the yaw angular rate,
ϕ – the pitch angle,
θ – the roll angle,
ψ – the yaw angle,

CHAPTER 4

LQR DESIGN FOR ATTITUDE STABILIZATION

In this study, the attitude stabilization is aimed. For this purpose the chosen controller is LQR. In order to use LQR the nonlinear system at hand must be linearized around a certain operating point. For this purpose, the jacobians of the nonlinear state equations are derived with respect to the states and the inputs. In this way the state space matrices A, B, C, and D are obtained after substituting the operating point state values. The controllability of the physical system is examined by checking the controllability matrix and it is found to be fully controllable for all 12 states (see Appendix 1). Attitude dynamics of the system is completely observable with the utilized sensor set. Observability analysis is also carried out by checking the rank of observability matrix (see Appendix 1). Therefore those states governing the attitude of the system could be controlled with the chosen sensor set.

4.1 Linear Quadratic Regulator

Linear quadratic regulator is a widely used modern control technique. It is preferred because of its easy implementation and its optimality for linear time invariant systems. It is an optimal and robust technique for Multi Input Multi Output (MIMO) control. Using this method the optimal control feedback coefficients are derived, the derivation of which is given in the following lines.

Given a linear time invariant system in state variable form as [15];

$$\begin{aligned} \dot{x} &= Ax + Bu \\ y &= Cx + Du \\ x(0) &= x_0 \end{aligned} \tag{58}$$

where x is the states of the system, u is the input, A is the system matrix, B is the input matrix, C is the output matrix and the D is the direct transition matrix. LQR controller tries to minimize the performance index given as;

$$J(u)=\int_0^\infty y(t)^T y(t)dt$$

$$J(u)=\int_0^\infty \left(x(t)^T C^T Cx(t)+u(t)^T D^T Du(t)+2x(t)^T C^T Du(t)\right)dt \tag{59}$$

Where the above given equation terms can be replaced with their equivalents as;

$$\begin{aligned} C^T \cdot C &= Q \\ C^T \cdot D &= S \\ D^T \cdot D &= R \end{aligned} \tag{60}$$

$$J(u)=\int_0^\infty \left(x(t)^T Qx(t)+u(t)^T Ru(t)+2x(t)^T Su(t)\right)dt \tag{61}$$

The linear solution that minimizes this index is given by some linear function of states;

$$u=-Kx \tag{62}$$

and the feedback gain is given as;

$$K=-R^{-1}\left(B^T P+S^T\right) \tag{63}$$

After the required substitutions are done, the feedback gain matrix for the system is;

$$K=\begin{bmatrix} 0 & 5.9581 & -2.2495 & 0 & 7.0711 & -2.2361 \\ 6.0097 & 0 & 2.2495 & 15.8114 & 0 & 2.236 \\ 0 & -5.9581 & -2.2495 & 0 & -7.0711 & -2.236 \\ -6.0097 & 0 & 2.2495 & -15.8114 & 0 & 2.236 \end{bmatrix} \tag{64}$$

Linear quadratic regulator solves also a Ricatti equation given as;

$$A^T P+PA-\left(PB+S\right)R^{-1}\left(B^T P+S^T\right)+Q=0 \tag{65}$$

where P is the stabilizing solution to the Ricatti equation [15].

$$J=\int_0^\infty y(t)^T y(t)dt = {x_0}^T Px_0 \tag{66}$$

In the above equation (66), Q is the state control matrix and it is important when defining which states are more important and which are less important. It means that, larger values of Q generally results in the poles of the closed loop system being left in the s-plane so that the states decay faster to zero. On the other hand, R is the performance index matrix also referred as the cost of inputs. Experiments are done with different Q and R matrices to get the best response [15].

In Figure 21 the change in six states can be seen during LQ regulation for both the nonlinear and the linear state space model (Figure 20). All states are regulated to zero in both systems.

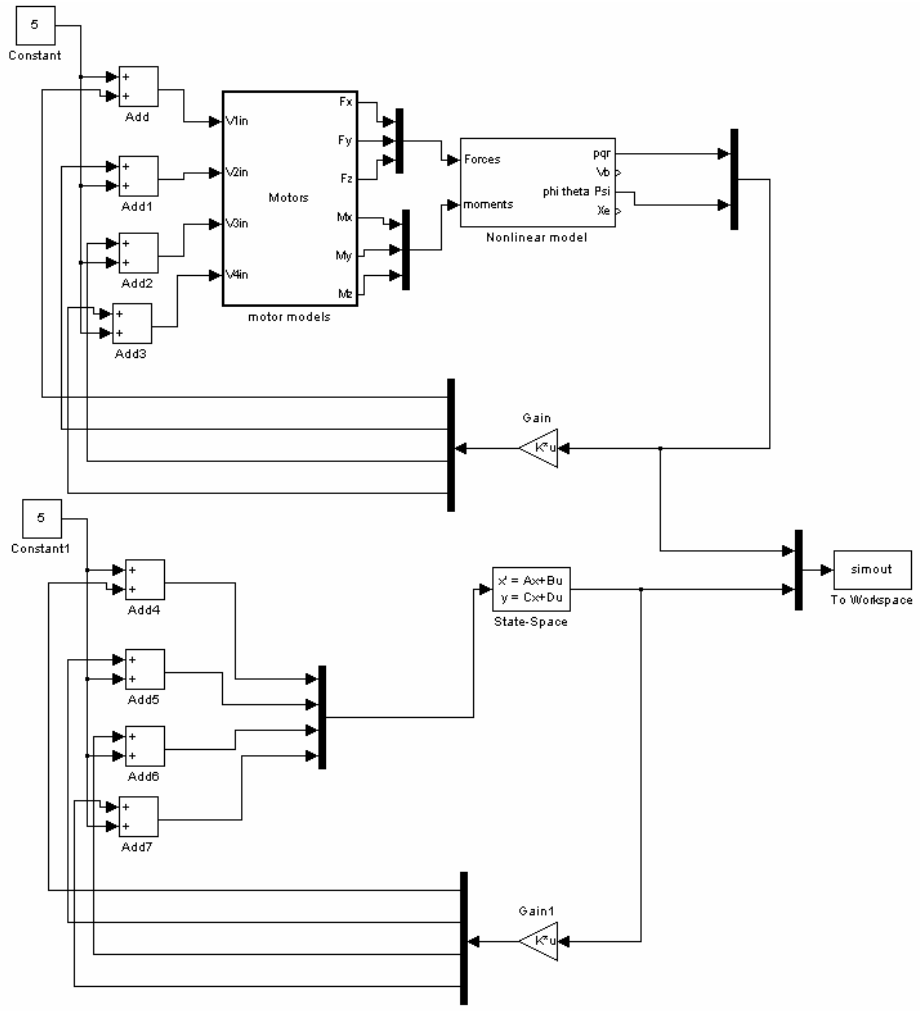

Figure 20 The LQR system for nonlinear and linear state-space models

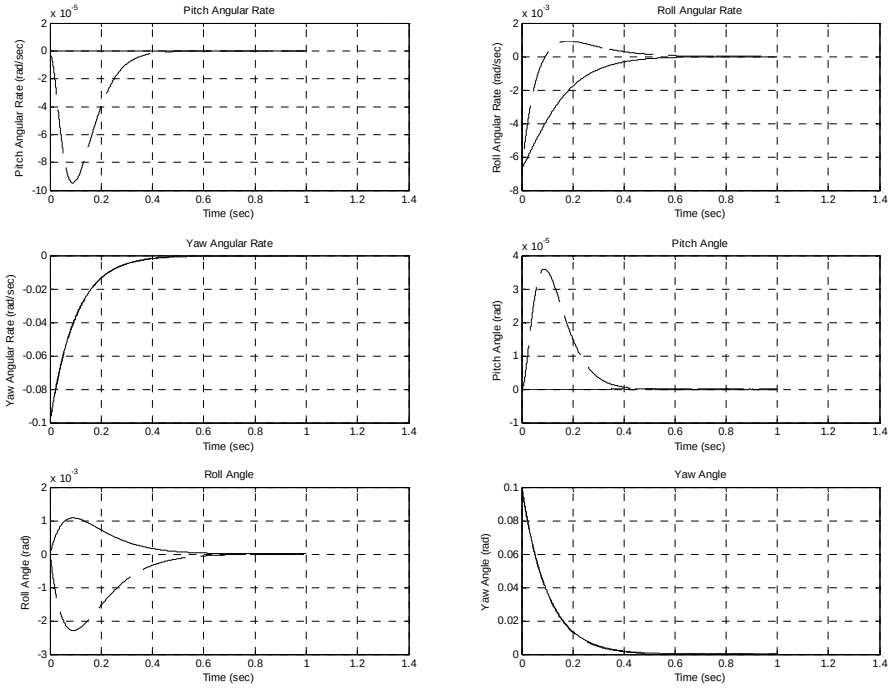

Figure 21 Comparison of the nonlinear and state space models for a 0.1 rad disturbance in yaw angle (continuous line represents the State space model and dashed line represents nonlinear model)

CHAPTER 5

STRUCTURE AND TEST BENCH

This chapter discusses the hardware used in the development of the quadrotor. The commercially available hardware components have been used in this research. Steps of the physical integration of the system have been discussed in this chapter.

5.1 The Frame of the Quadrotor

For the body of the quadrotor the frame of the commercial quadrotor named DraganFlyer Vti model is used. The frame composed of carbon tubes attached with a plastic hub from their ends forming a plus shape. At the other ends of the carbon tubes motor-propeller assemblies are attached. The 15 cm carbon tubes are used because of their light weight (4 g) and high stiffness properties. Total frame assembly weighs about 270 g without any electronic hardware. Instead of the original electronic circuits a custom board has been designed and attached on board later.

5.2 Sensors Used in the System

The sensor alternatives (Figure 22) (Table 2) that can be used in this study are Murata ENC03 gyros, Silicon Sensing CRS02 or CRS04 gyros, Honeywell magnetometer and Parallax compass module, Memsic accelerometers and Analog devices accelerometers, which are also available in our Robotics laboratory.

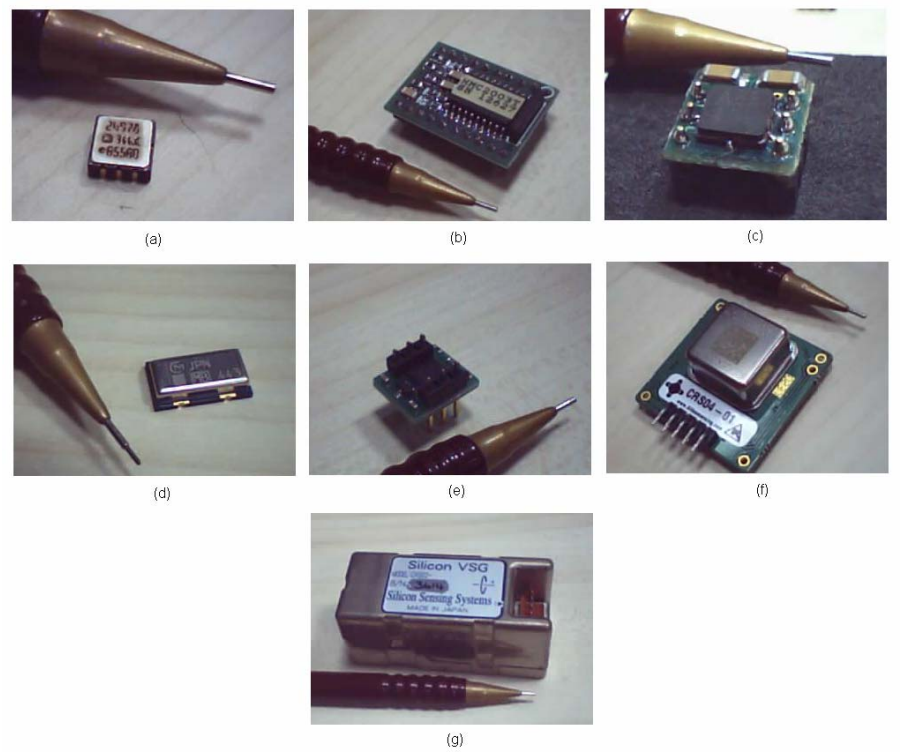

Figure 22 (a) Accelerometer (Analog devices) (b) Magnetometer (Honeywell) (c) Accelerometer (Memsic) (d) Gyroscope (Murata) (e) Compass Module (Parallax) (f) Gyroscope (Silicon sensing) (g) Gyroscope (Silicon Sensing)

Table 2 Available Sensors

Analog devices	ADXL203EB	Dual Axis Accelerometer
Analog devices	ADXL202	Dual Axis Accelerometer
Analog devices	ADXL311	Dual Axis Accelerometer
Analog devices	ADXRS300ABG	300deg/s single chip rate gyro
Analog devices	ADXRS150ABG	150 deg./sec. angular rate sensor
Honeywell	hmc 1023	3-axis magnetometer
Honeywell	Hmc 2003	3-axis magnetometer
Honeywell	Hmr 2300R-485	3-axis magnetometer
Honeywell	Hmr 3000-demo-232	Compass module

Honeywell	Hmr 3200-demo-233	Compass module
Honeywell	Hmr 3300-demo-234	Compass module
Parallax hitachi	HM55B	Compass module
Murata	ENC 03	Angular rate gyro
Silicon sensing	CRS04c	Single axis angular rate sensor
Silicon sensing	CRS02c	Single axis angular rate sensor
memsic	MX2125	low cost, dual-axis thermal accelerometer

Most of the sensors at hand provides digital outputs, which requires additional hardware to transmit data to the PC terminal. In addition to that some digital output sensors have low resolution results. For example, parallax HM55B compass module has 11 bit resolution with a 20 ms conversion time. Because of these deficiencies instead of digital output sensors, analog output sensors are chosen. ADXRS150 EB Gyro evaluation board, ADXL203 accelerometer module and HMC2003 3 axis magnetometer modules are used. Their properties are further discussed in the below topics.

5.2.1 Accelerometer

Analog devices ADXL203 accelerometer (Figure 23) was used to measure the roll and pitch angles of the system. In order to do these measurements it was worked in tilt measuring mode.

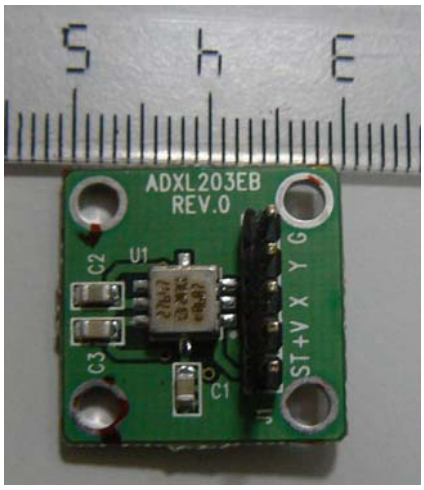

Figure 23 Accelerometer (ruler is in centimeters)

The accelerometer evaluation board (Figure 24) is factory-set for a bandwidth of 50Hz which is higher than the required filter frequency. In order to obtain a proper bandwidth, the outputs of the sensor are filtered using 1 μF capacitors. These capacitors work as low pass filter with cutoff frequency of 5 Hz [42].

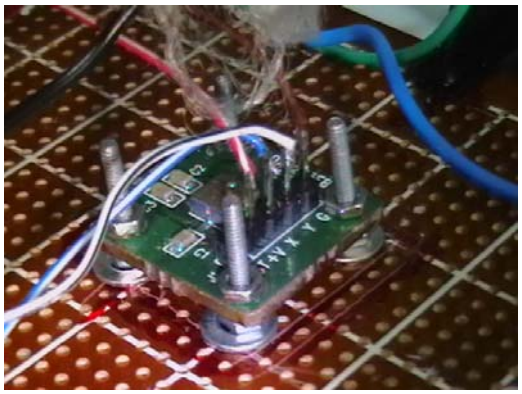

Figure 24 ADXL203EB accelerometer evaluation board

The accelerometer measures the tilt angles, which are assumed to represent the Euler angles. Therefore, unlike the gyroscopes, that measure only the angular rates, the tilt sensor placed as close as possible to the center of gravity. The mounting was done on to the lower PCB's center as shown in the Figure 24 using 2 mm screws.

5.2.2 Gyroscopes

Three Analog devices MEMS Gyroscopes (model ADXRS150) were used in the system. These gyros are soldered on an evaluation board, like the one shown in Figure 25. These evaluation boards weigh three grams each, and are about 2,54 cm long by 1.27 cm wide and costs $50. The chip on this board is also available from Analog Devices Inc. However; the evaluation board does not require any external resistors or capacitors for the gyroscope to be used. Also, the gyroscope's ball grid array chip connections, which are difficult to solder by hand, have already been soldered onto the evaluation board.

The sensor uses a resonator gyro that senses Coriolis motion and is capable of measuring +/−150 degrees per second of angular velocity. The chip produces an analog voltage output (between 0.25 and 4.75 V for a 5 volt source) that is proportional to the angular velocity about the axis normal to the top surface of the gyroscope package. The voltage increases for clockwise rotation (while looking down at the top of the chip) of the gyroscope. The noise density of the gyroscope, which is defined as the average noise at any frequency (f, in Hz) in the bandwidth of the part, is 0.05 ^{o}/sec/pF. The initial null point is 2.5 V, but this can change by a maximum of 300 mV for a temperature range of −40 to 85^{o}C. The sensitivity of the gyroscope varies from 11.25 to 13.75 mV per degree per second over the gyroscope's operating temperature range. The gyroscope includes signal conditioning electronics to help preserve the signal in noisy environments. The bandwidth of the surface mount gyro chip can be set using external resistors and capacitors.

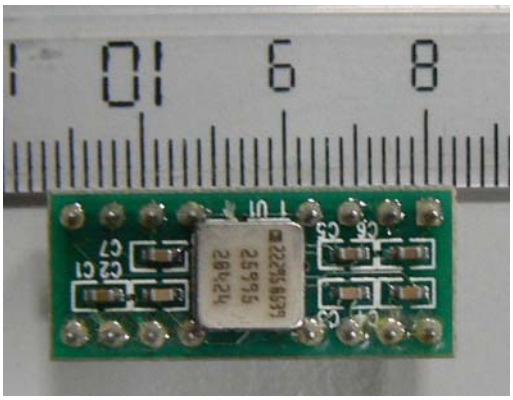

Figure 25 A picture of the gyroscope evaluation board ADXRS150EB (ruler is in centimeters).

The bandwidths of the gyros are factory-set at 40 Hz (Figure 25). Each one of the gyros was placed on different PCBs which are perpendicular to each other like the one shown in the Figure 26. The axis of measurement of the gyro is pointing out of the paper in Figure 25. Therefore in order to measure angular rates around three orthogonal body axes the gyros were placed such that their axis of measurement stayed parallel to the corresponding axes of rotation (Figure 26).

5.2.3 Magnetometer

Honeywell HMC2003 model 3 axis magnetometer was installed on to the PCB. It is shown in the Figure 26 with an arrow. Magnetometer gives analog voltage outputs proportional to the magnetic field along each orthogonal body axis. In this configuration the magnetometer is used only to measure the yaw angle around the earth-fixed vertical axis. Since the system's attitude is stabilized near hovering, only one axis measurement of magnetometer is utilized, which is the horizontal axis.

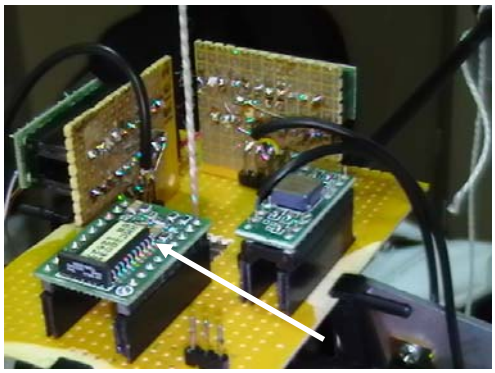

Figure 26 Magnetometer at the lower left corner and three gyros at the back of it (magnetometer shown with an arrow)

On the sensor board there are three orthogonal MEMs gyroscopes (ADXRS150-Analog devices), one Magnetometer (HMC2003-Honeywell) and a voltage regulator ic (7805). The circuit diagram for the sensor set is given in Figure 27.

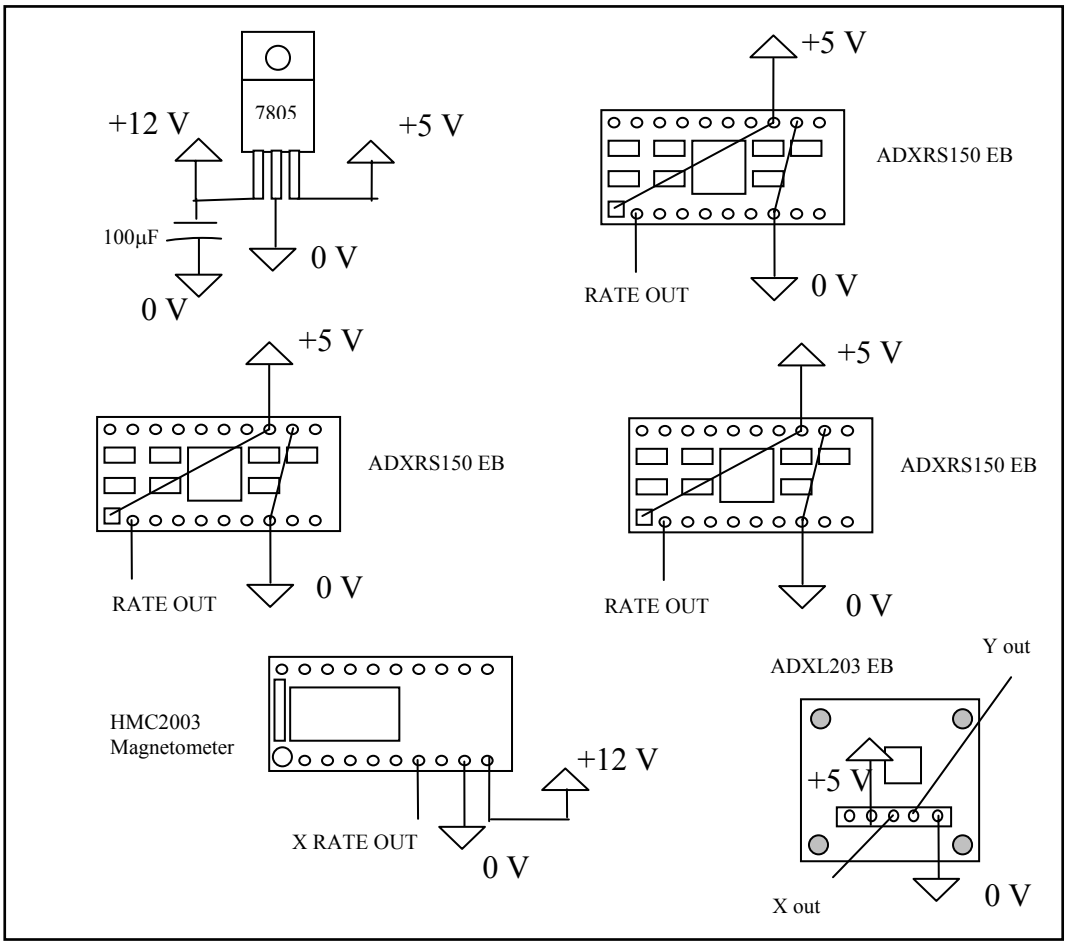

Figure 27 Circuit diagram of the gyro hardware

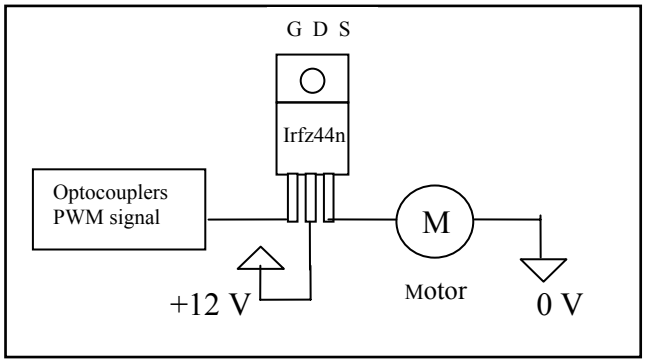

Figure 28 IRFZ44N n-channel Mosfet transistor schematic for motor drivers

There is another circuit board beneath the gyro board that is carrying four n-channel mosfet transistors. These transistors are the motor driving transistors. The schematic for a single n-channel Mosfet motor driver is shown in Figure 28.

5.3 Drivers

In Draganflyer Vti model four mosfet transistors model iflz44n are used and are driven in switching mode with a 5 V PWM signal which has a frequency of 178 Hz [23] (Figure 29).

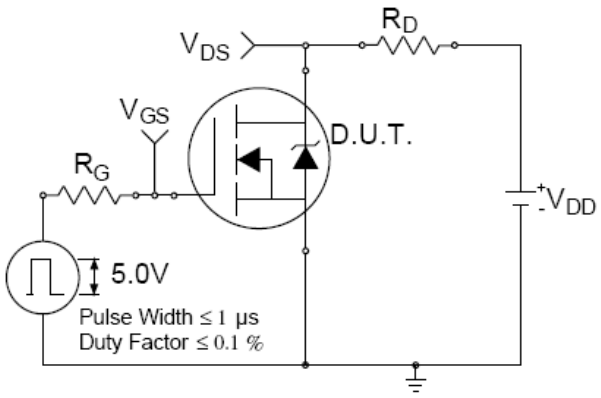

Figure 29 Mosfet IRLZ44N driven in switching mode [34]

Mosfet's input impedances are very high whereas their on resistances are very low (around 0.022 Ω). These properties are desired on motor driver applications where high currents are needed. In high current conditions the energy dissipation on the transistor increases with the increase in their on resistances. So the more the resistances are the more it dissipates heat, which may cause changes in the behavior of the transistor [33].

PWM driving technique is more efficient and easily produced with logic circuitry such as microcontrollers, which makes it the proper choice for driving the motors at hand. [35]

Logic level gate drive mosfets are suitable for directly connecting them to microcontrollers and other logic ic's. This property prevents the usage of other gate driving integrated circuits. For instance, draganflyer Vti model uses IRLZ44 logic level gate drive mosfets.

There are some readily available motor drivers. Such as simple H bridge motor driver [37].Unfortunately this driver doesn't include isolation for noise. And the motor voltage is in the range +6 V and +36.0 V range, which is outside the voltage range of our motors. Alternatively there are other readily available speed controllers such as Astro flight 204D speed controller [36] [35]. This controller (Figure 30) is designed for large Cobalt Motors. It is rated at 60 amps at 60 V, so it can handle large motors like the Cobalt 90 motor. It can also be used with other cobalt or ferrite brushed motors.

The 204D has optocoupler on the input to reduce chance of radio interference from conducted motor noise. There is a built in voltage doubler for solid MOSFET drive and the control is all digital using a special micro processor.

The four 80N06 mosfets used in the motor drive circuit have a combined resistance of less than 2 milliohms. This low resistance lets the control run cool and gives the 204D control a continuous current rating of 50 A.

Figure 30 ASTRO 204D speed controller

5.4 Proposed Driver Circuitry

There are four blocks in the design (Figure 31). The first block is the data acquisition card block which helps the communication with the computer through its terminal board (Figure 32) (Figure 33). The sensor signals are coupled to the terminal board's analog inputs via 10 kΩ resistors (Figure 32) to reduce noise levels and also reduce any excessive current leakage from the sensors' low fan out outputs. The second block is the processor block, which includes two 16F877 microcontrollers on it. Each processor is capable of converting two analog signals to two PWM signals. Therefore at the output of this stage 4 PWM signals at 0-5 V level is obtained (Figure 35).

The PWM signal generated by the PIC16F877 microcontrollers has a period of 4.3 ms and a frequency of 232.6 Hz with a 10 bit resolution A/D conversion and PWM generation [38]. The higher frequency PWM signals create noise in the motors and an efficiency loss, which are undesirable [39].

5 V PWM signals are fed into the optocoupler and mosfet driver stage (Figure 36). In this stage the 0-5 V PWM signal is converted to a 0-10V isolated PWM signal which is the required signal level for driving the mosfets in switching mode.

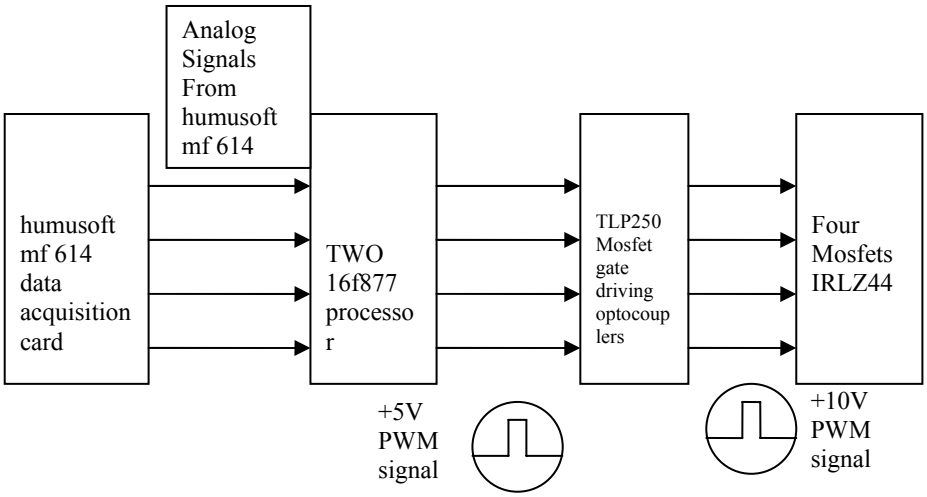

Figure 31 Driver system block diagram

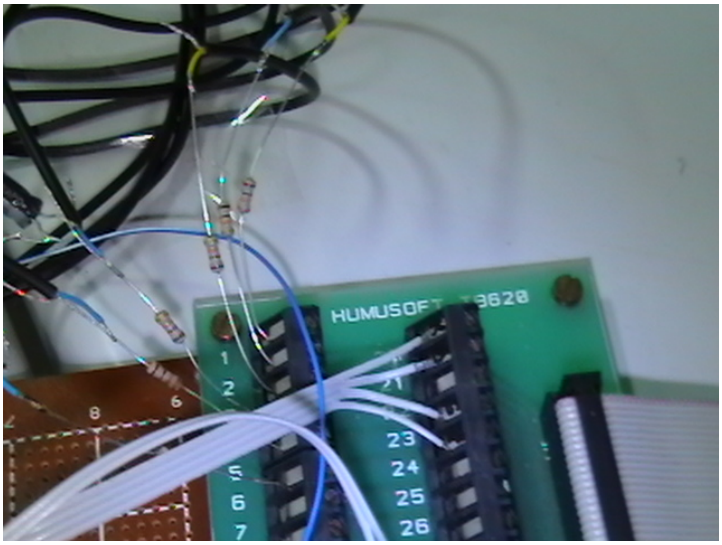

Figure 32 Terminal board

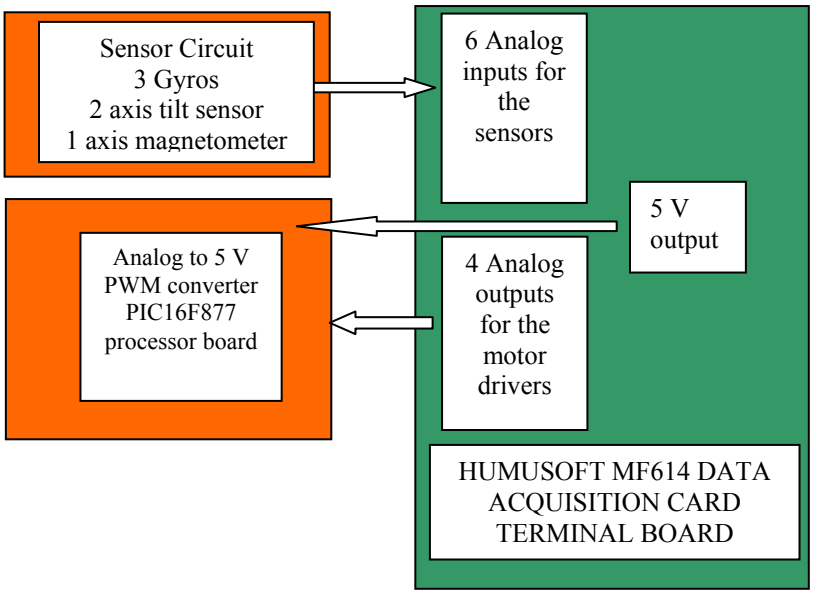

Figure 33 The Block diagram for the data acquisition card terminal board

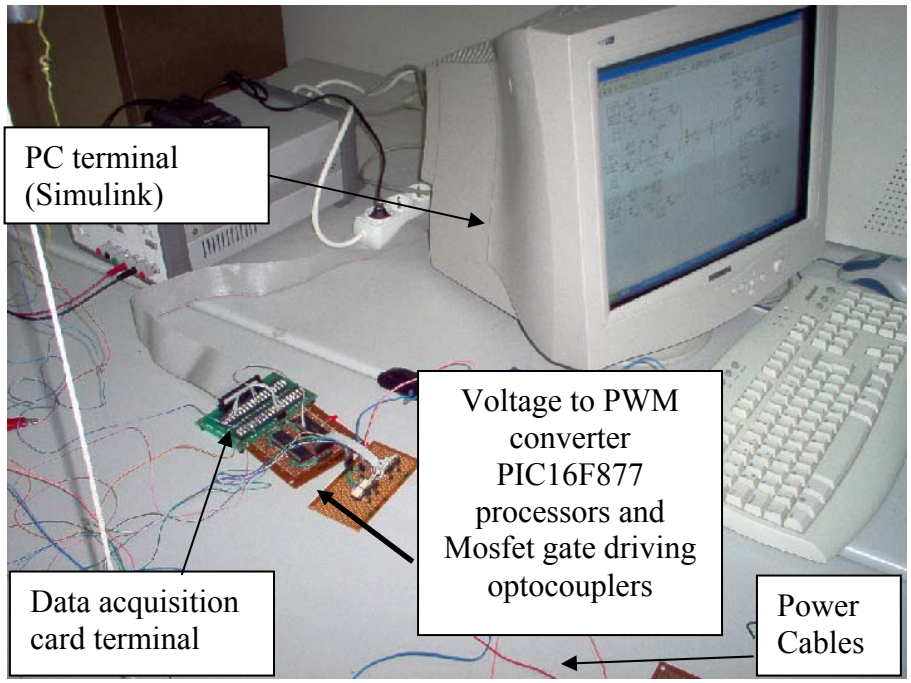

Figure 34 A view of the hardware system

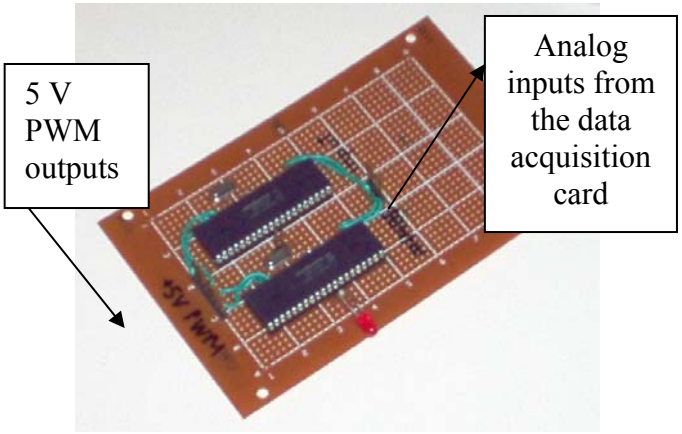

Figure 35 Voltage to 5 V PWM converter

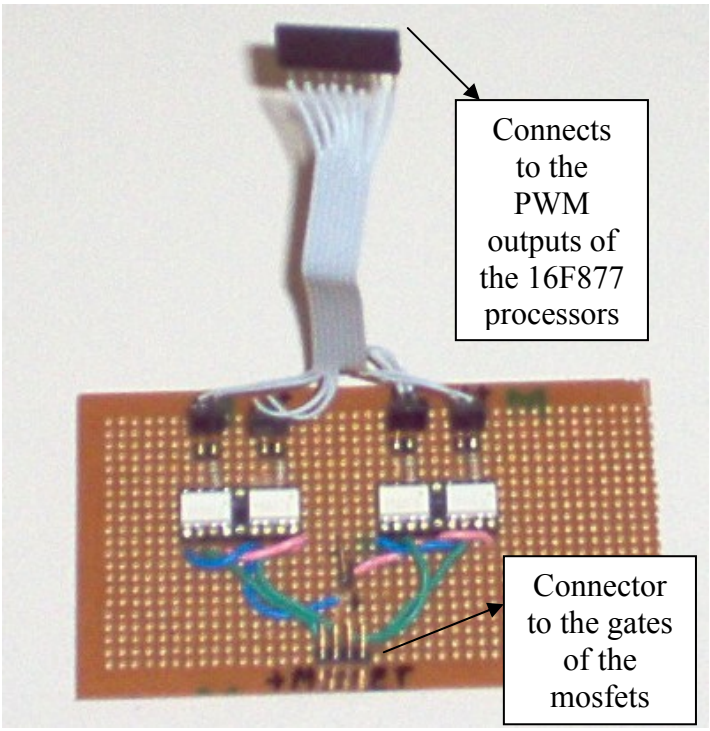

Figure 36 Mosfet gate driving optocouplers (TLP250)

TLC250 optocouplers (Figure 36) provide both mosfet gate driving and isolation from motor circuitry, which prevents noise entering into the data acquisition board [35].

IRFZ 44N is the preferred mosfet transistor for driving the motors. It can be driven with a 10 V PWM signal, which is suitable for the system at hand [34].

The wires and connections made to the system effects the model of the system so in order to minimize these effects the motor drivers are placed on board so that the thick power cables are confined into the hardware onboard. Therefore only the signal cables are extended from the body of the quadrotor.

The power mosfets are attached to properly sized heat sinks (Figure 37) and placed closer to the outside corners of the PCB in order to dissipate the heat away easily with the help of the air flowing due to the rotation of the propellers. The characteristics of the mosfets change with their temperature so keeping their temperature constant is paramount while they are working.

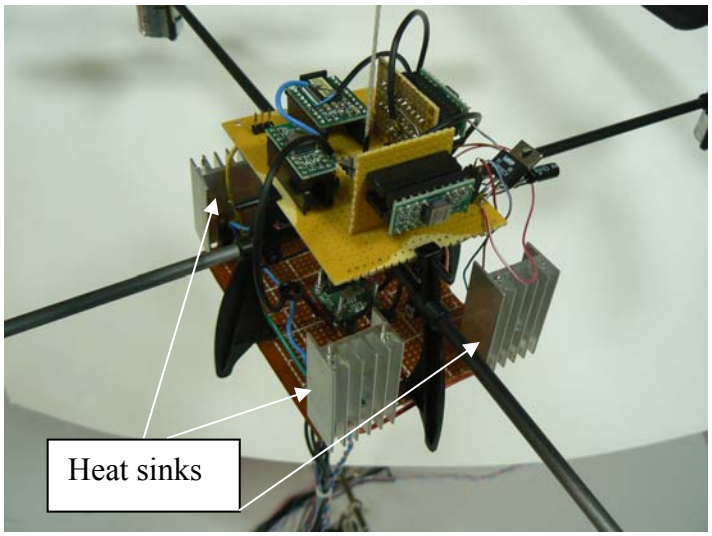

Figure 37 Electronic Hardware

In the experiments motors created high back emf voltages which when driven with transistors may damage the mosfet transistors. So in order to eliminate these high reverse voltages a small 22nf capacitor is placed between two terminals of each motor (Figure 38). So when a high reverse voltage is created it is shorted through this bypass capacitor.

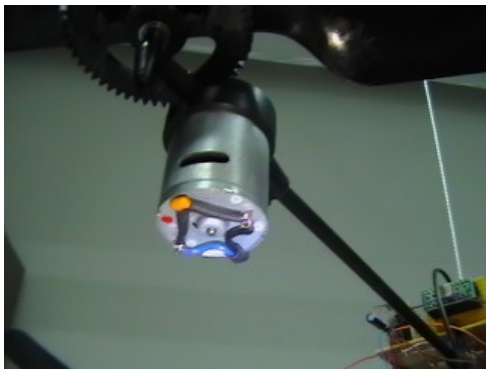

Figure 38 By-pass capacitor for high reverse inductive voltages

5.5 Power Supplies

The Agilient 6653A power supply (Figure 39) is used in the setup as an energy source for the motors. It can supply 15 amperes at most at 35 V which is sufficient for the system at hand. The system needs 10 amperes at most at 12 V. The switching power supplies created noise in the sensor outputs so, instead of using AC connected switching power supplies 12 volt lead acid battery is used to supply for the sensor set (Figure 40).

Figure 39 Agilient 15 A / 35 V Power supply

Figure 40 Power supply for the sensor set

A button is placed near the PC terminal. In case of an emergency situation it cuts the power going to the system as it is pressed (Figure 41).

Figure 41 emergency button

5.6 Driver Test Results

Mabuchi DC motors of the system are tested after they are connected to the mosfet driver stage. PWM test result can be seen in the Figure 42 for the proposed controller.

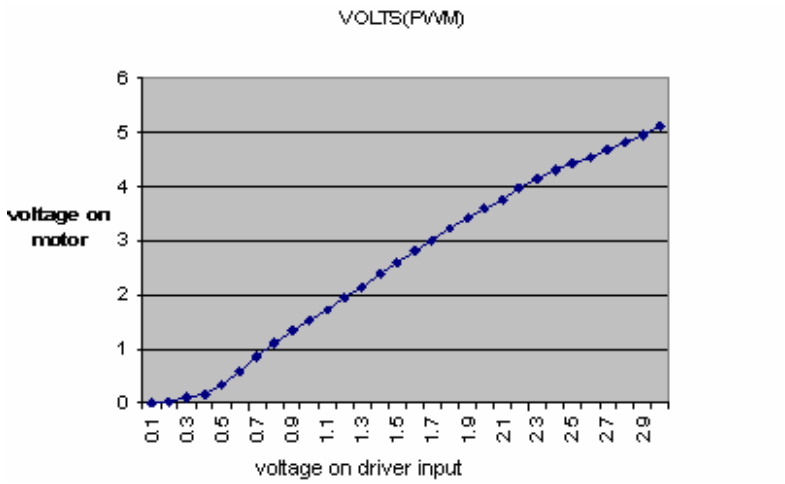

Figure 42 PWM driven Mabuchi motor's RMS voltage

The behavior of the driver is nonlinear (Figure 42). In order to use this data a polynomial function is fitted to the test data. Then this polynomial function is used in the Simulink model to obtain the proper motor voltages.

5.7 Test Bench

After all the parts are assembled together the final system looks like the one shown in Figure 43.

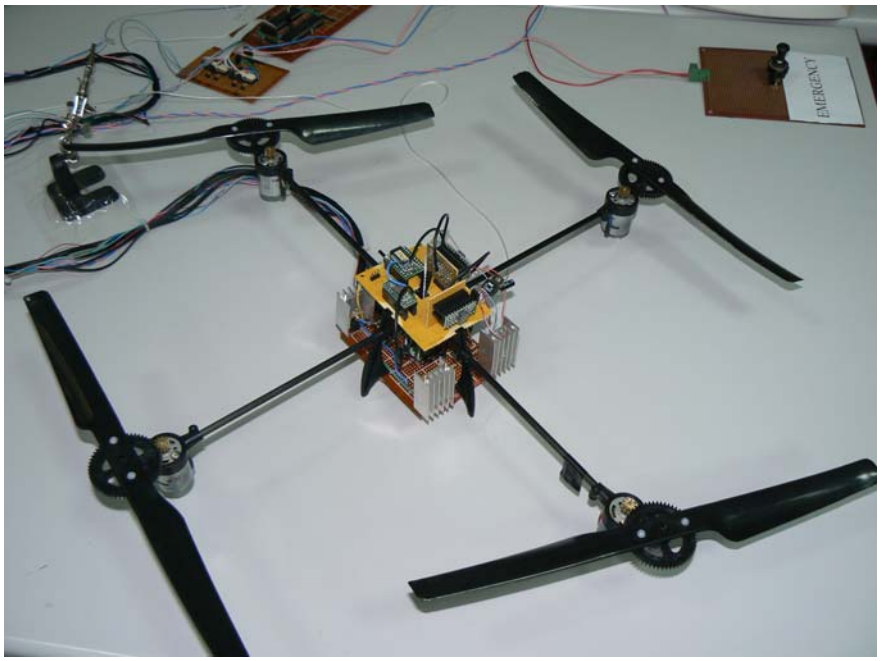

Figure 43 Assembled Quadrotor

After the quadrotor assembly finished the options of experimental setup is considered. One of them is hanging up the quadrotor body with a rope. This keeps the system at a constant height. The two other translations and the three orientations are free. However this setup has a disadvantage. When the system sways side ways the connected rope creates a decoupling action which stabilizes the overall system to certain extend [19] (Figure 44) (Figure 45).

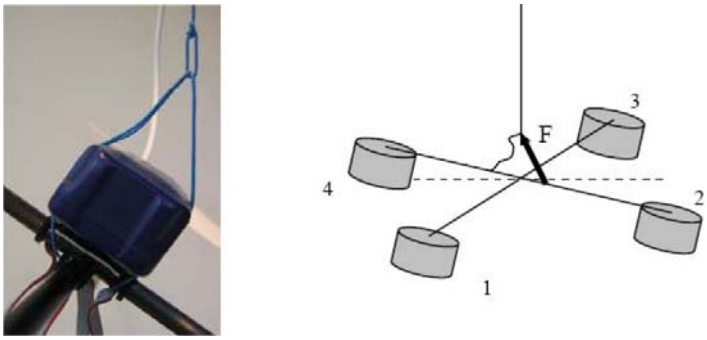

(a) (b)

Figure 44 Cable connection

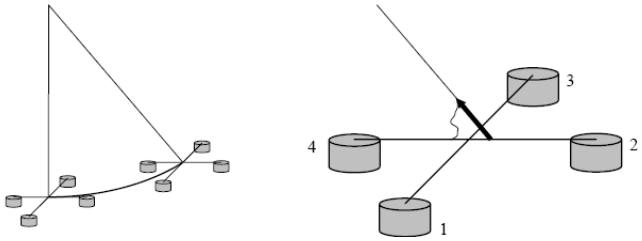

(a) (b)

Figure 45 Side sways

Another option of experimental setup is the one which has a spherical joint (Figure 46) [19]. It prevents the three translations but not three rotations.

Figure 46 The kneecap or spherical joint

The available spherical joints tested but their friction rates found to be effectively high. Finally, rope assembly decided to be used in the test bench. But it was not connected to the quadrotor frame with an offset like it was in Figure 44. Instead the rope passed through an opening in the top PCB gyro board (Figure 48) and connected to the center of the cross frame, which reduced the couples that had been caused when an offset was given to the rope-frame connection.

Figure 47 Experimental setup

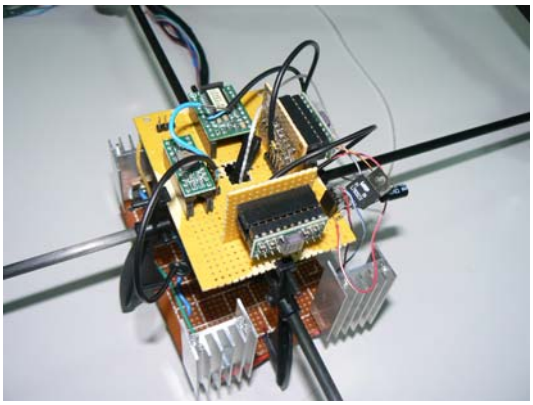

Figure 48 The hole at the centre of PCB

The final system is hanged with a rope from the center of gravity (Figure 47). And each motor end is loosely supported with ropes in order to prevent large, uncontrolled sways and establish safety during working.

The bundle of signal cables that are extended from the quadrotor are winded together and extended close to the axis of center of gravity in order to reduce the torques created by the wires.

CHAPTER 6

REAL TIME CONTROL IMPLEMENTATION

The control software is implemented in Matlab/Simulink. The Real Time Windows Target and Real Time Workshop of the Matlab are utilized while controlling the hardware in the loop system. The data acquisition card that is used for this purpose was Humusoft MF614.

Humusoft MF614 data acquisition card has four analog output channels and eight analog input channels. Drivers for Real-Time Windows Target, xPC Extended Real Time Toolbox for MATLAB and drivers for windows are included. It also has four quadrature encoder inputs (differential). Additionally, it has eight digital inputs and outputs.

6.1 The Control Software

The control algorithm consists of several different stages. First stage is the data acquisition stage. In this stage the information about the orientation of the quadrotor are acquired from the sensors. In the second stage the orientation information is multiplied with the LQR gain matrix. In the third stage the motor signals coming from the LQR controller are sent to the motor drivers.

In the data acquisition stage the raw data (in volts) from the sensors are acquired via the data acquisition card. In Simulink this job is done with an Analog input block present under the Real-Time Windows Target library. The raw data obtained by the Analog input blocks are the sensors' outputs in V where as the data required by the LQR controller must be in radians for the angles and radians per second for the angular rates. In order to convert these raw voltage signals into proper units conversion blocks are placed at the outputs of the Analog input Blocks. In Figure 50 the conversion block is shown on the right. In addition to the conversion block an offset calibration block is also placed at Analog input block output in order to use for

later calibrations. Calibration block consists of a constant subtracted from the sensor output signal (Figure 50).

In the second stage the orientation information obtained in the first stage is multiplied with the LQR gain matrix K. The derivation of K matrix was given in Chapter 4.

In the third stage the LQR control signals are output to the external motor driver circuitry via the data acquisition card. In Simulink this job is done with an Analog output block present under the Real-Time Windows Target library. The control signal passes through some other Simulink blocks before it is outputted via the final Analog output block. In Figure 49 LQR Motor signal block can be seen on the left. This block links the LQR controller to the converter1 block which adjusts the signal such that the voltage value ordered by the controller is seen on the motors. Then the output of this converter block is added with an adjustable motor voltage reference for thrust adjustment i.e. if the thrust of all four motors wanted to be increased the slider gain block in Figure 49 can be used to increase the voltages on the motors. After the summation operation the motor signal passes through a saturation block which avoids voltages higher than 5 V and lower than 0 V to be given to the driver circuitry. And finally the motor signals are outputted to the external driver circuitry via the Analog Output Block as shown in Figure 49.

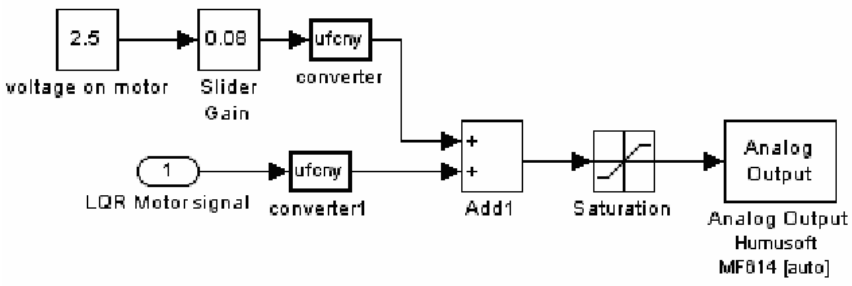

Figure 49 Simulink blocks for one motor

6.2 Calibration of Sensors

In order to get the accurate orientation information the sensors they must be calibrated well before the system is worked. The first thing to calibrate is the voltage outputs of the sensors. For instance although the same model gyros are used in the

sensor set, their outputs are quite different from each other when they are tested in still position.

So the first thing that should be done is to offset their output values such that they all give zero output at still position. This is done using the calibration constant mentioned in Figure 50.

In order to determine these offset values system is prepared for a calibration. System kept still initially and leveled horizontally. The still position is important because the voltage outputs of the gyros at 0 angular rates were required. During hovering these voltage values are necessary to keep the attitude stable. For instance if a wrong voltage value were assigned for zero angular rate value it would mean that the sensor will see the system as not moving but the real system would be rotating with the angular speed corresponding to the voltage output of the gyro.

After the system had been made still the output of the gyros were read for 100 seconds and then the mean of this signal were taken to find the approximate voltage level corresponding to the zero angular rates. In Simulink this constant voltage value is subtracted from the signal to offset the signal output to zero value as mentioned before (Figure 50). The same steps are also repeated for the other sensors (Figure 51, Figure 52).

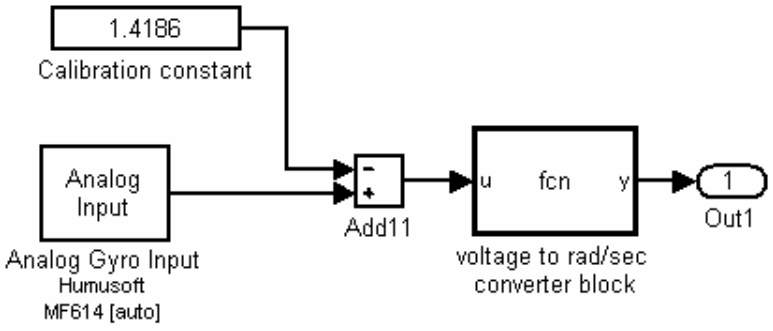

Figure 50 A Sample Gyro Block

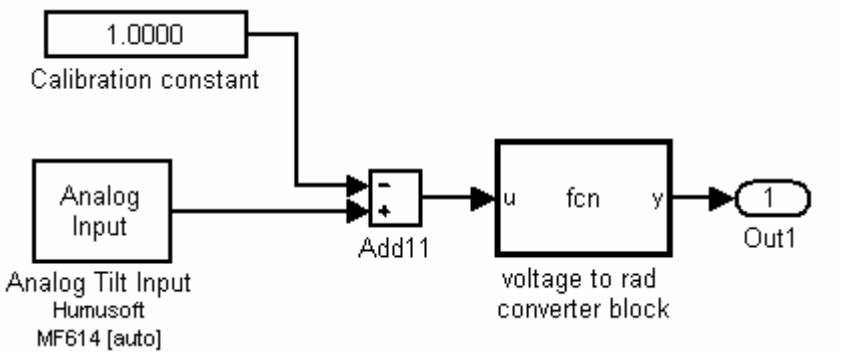

Figure 51 A sample accelerometer block

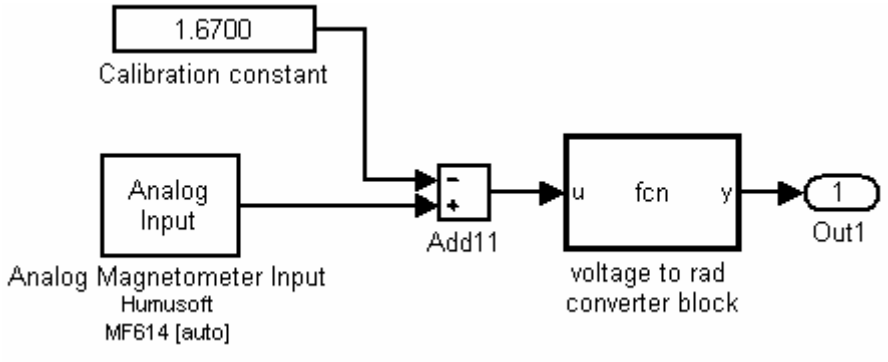

Figure 52 A sample magnetometer block

Table 3 Calibration constants (at room temperature ~20^0)

Sensor Name	Calibration constant
Gyro (p)	1.4186
Gyro (q)	1.4081
Gyro (r)	1.4201
accelerometer (ϕ)	1.0002
accelerometer (θ)	0.8600
Magnetometer (ψ)	1.6700

After the calibration of the sensors (Table 3) for level and no-motion case their maximum voltages at the limits are tested. For instance, the gyro Sensors that are used in the system give their maximum and minimum voltages at angular rates above 150 ^{0}/sec so, using these principles the gyros are given maximum angular rates

turning by hand. And using these tests the sensor output voltages at maximum angular rates are determined. The same thing is done for the tilt sensing accelerometers. The accelerometers give maximum and minimum voltage outputs at +/- 90^0 rotations. So, in order to determine those maximum and minimum voltage levels the system is turned by hand to +/- 90^0 angles both in pitch and roll angles. For the magnetometer the quadrotor is rotated around the vertical axis until the maximum and minimum outputs are distinguishable at the sensor output readings.

When converting the sensor outputs to the corresponding units it is assumed that the sensor outputs change linearly. So the equation representing this linearity had been found using the two critical points. For instance for a gyro first point is zero motion case at this point the angular rate is 0 rad/sec and the offset-voltage is zero. The second critical point is the maxima point. At this point the output voltage is some value and the angular rate is 2.618 rad/sec (150 ^{0}/sec) then a line fitting those two points is assumed to be the output equation of the gyros. On the other hand, the tilt sensing accelerometers measure the angles between -90^0 and +90^0. At level position tilt sensors should give zero output so that their maximum output corresponds to +90^0 of rotation and minimum output corresponds to -90^0 of rotation or vice versa (depending on the sign convention). So, a line can be fitted to those critical points to represent the output equation of the tilt sensors. The procedure for the magnetometer is the same as the tilt sensors' procedure. The only difference is that the rotation angle is around the vertical axis.

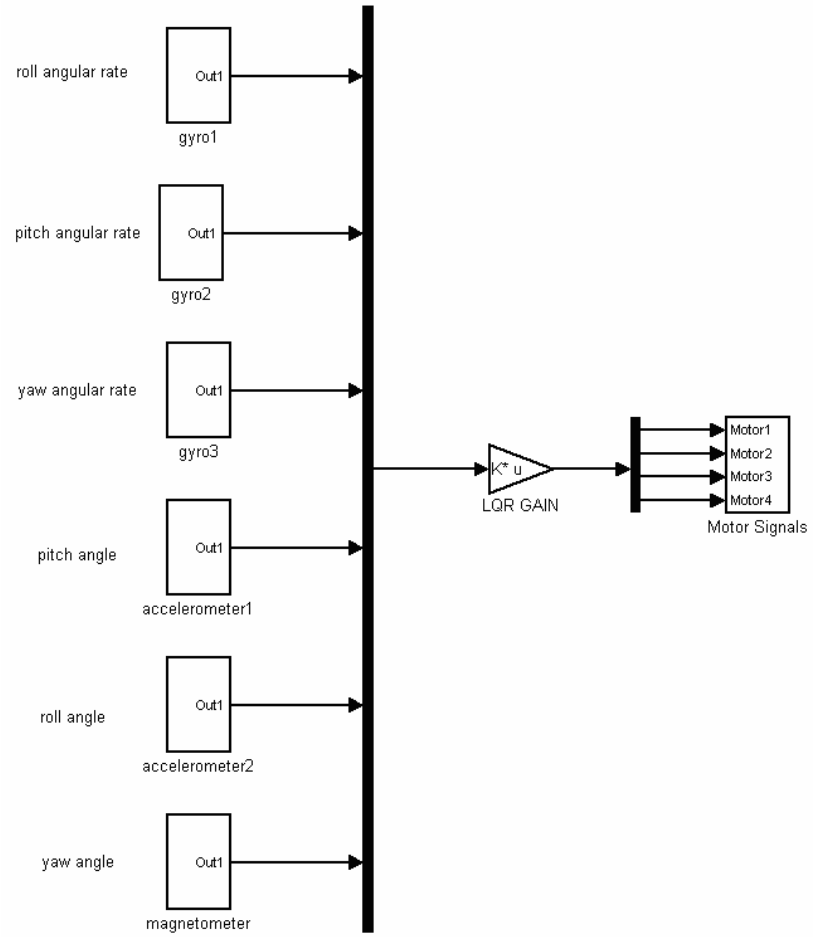

Figure 53 The Control Blocks in Simulink

Shortly, the signal information obtained from the sensors are acquired by the data acquisition card and then this information after processed fed to a LQR gain block, which outputs to the driver the controlling signals in volts. Figure 53 summarizes these software-implemented steps in Simulink. The signals sent to the driver are then converted to PWM signals by using some external hardware and given to the motor drivers. After this point on, these signals are able to conduct the control effort to the motors. The whole system is summarized in the block diagram given below (Figure 54).

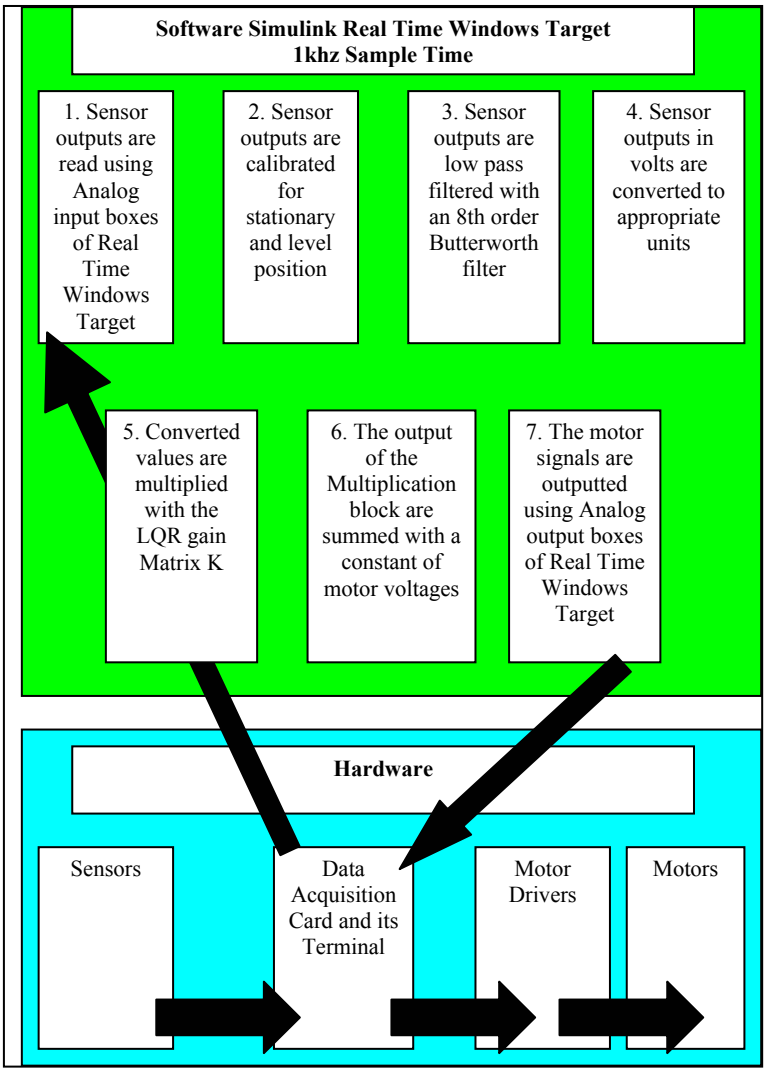

Figure 54 Hardware in the Loop System

CHAPTER 7

TESTS AND RESULTS

A robust system must have a good rejection of the disturbances and low sensitivity to the change in system parameters. In order to test the performance of the designed control system disturbances are given to the system along x, y, z axes. Tests have showed that the noise present in the sensor outputs degrade the controller performance. Therefore some precautions are taken for eliminating noise, which are discussed on the next title.

7.1 Eliminating Sensor Noise

Vibration Noise is intrinsically present in the accelerometers. In order to filter that noise 8th order Butterworth filters are placed at the outputs of the accelerometer in the simulink code. Before and after filtering of the accelerometer outputs are given in Figure 55, Figure 56, Figure 57 and Figure 58 after the system is disturbed physically. Note that the disturbance is given by pushing the system on x-y plane.

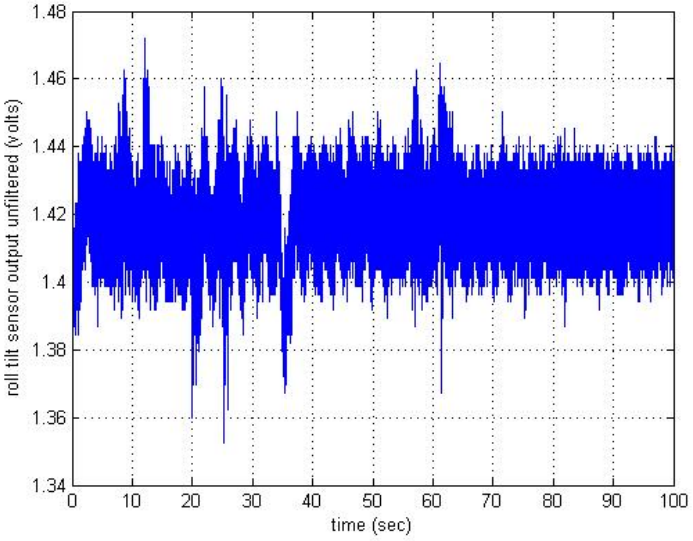

Figure 55 Unfiltered sensor output for roll angle

In Figure 55 it is clearly seen that the signal is almost disappeared under the noise. After the signal filtered with an 8th order Butterworth lowpass filter the signal becomes distinguishable and the pattern of motion can be seen (Figure 56).

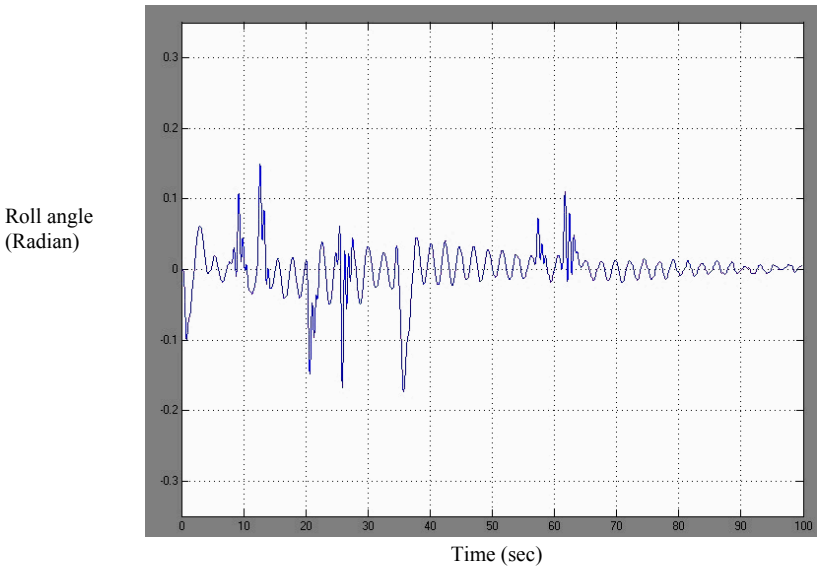

Figure 56 Filtered Roll angle measurement with a 8th order Butterworth lowpass filter with 10 Hz bandwidth

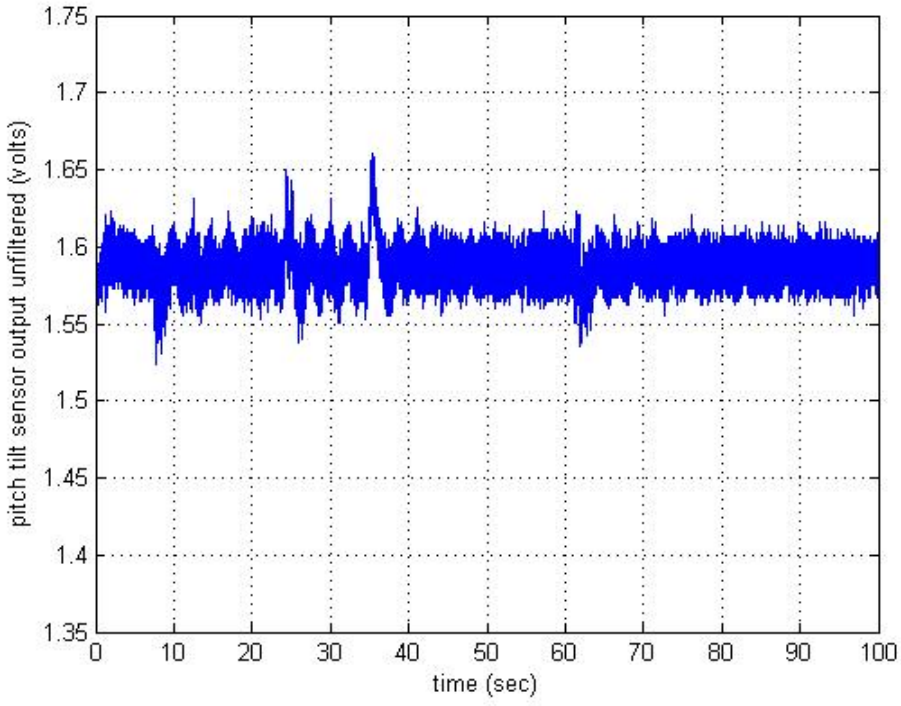

Figure 57 Unfiltered sensor output for pitch angle

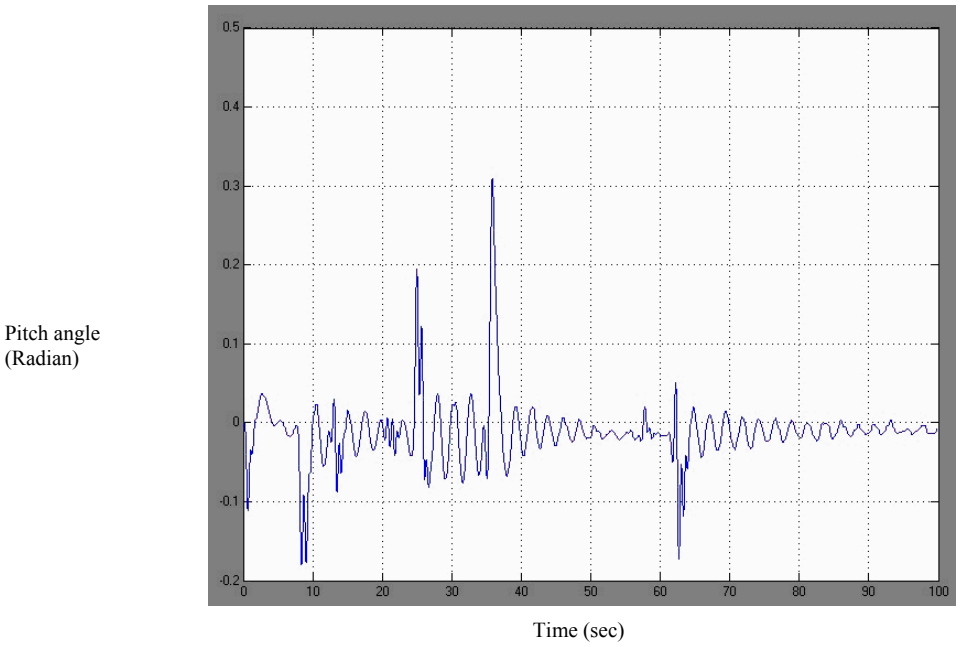

Figure 58 Filtered pitch angle with a 8th order Butterworth lowpass filter with 10 Hz bandwidth

For the same disturbance the outputs of the gyros are also given in the Figure 59, Figure 60 and in Figure 61 for yaw, roll and pitch angles respectively. It is important to note that all gyros have factory-set 40 Hz lowpass filter onboard.

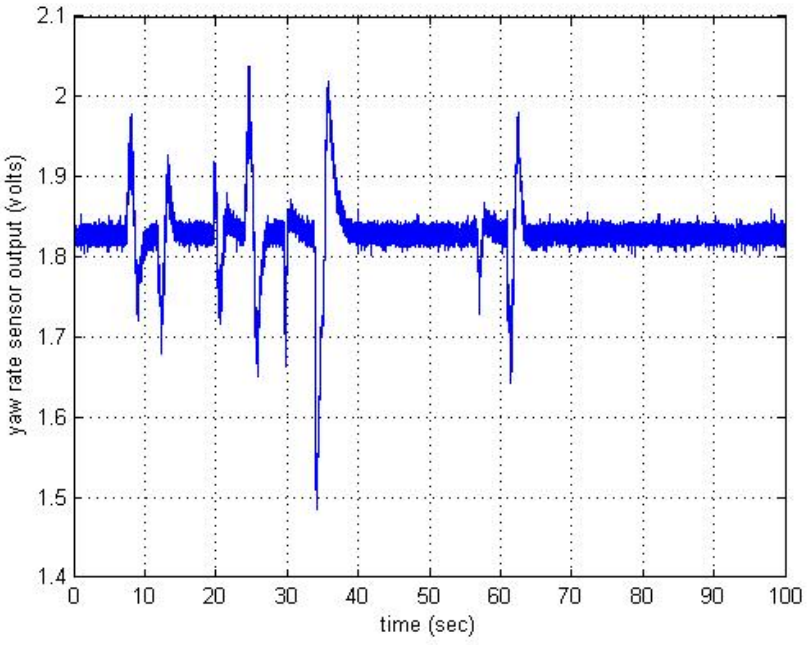

Figure 59 yaw rate unfiltered (only factory-set filter on the sensor) sensor output

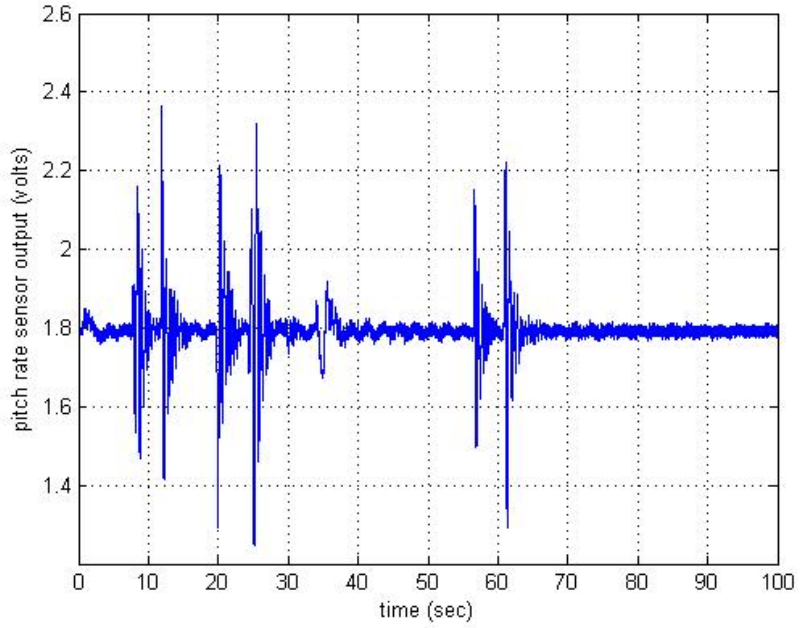

Figure 60 pitch rate unfiltered (only factory-set filter on the sensor) sensor output

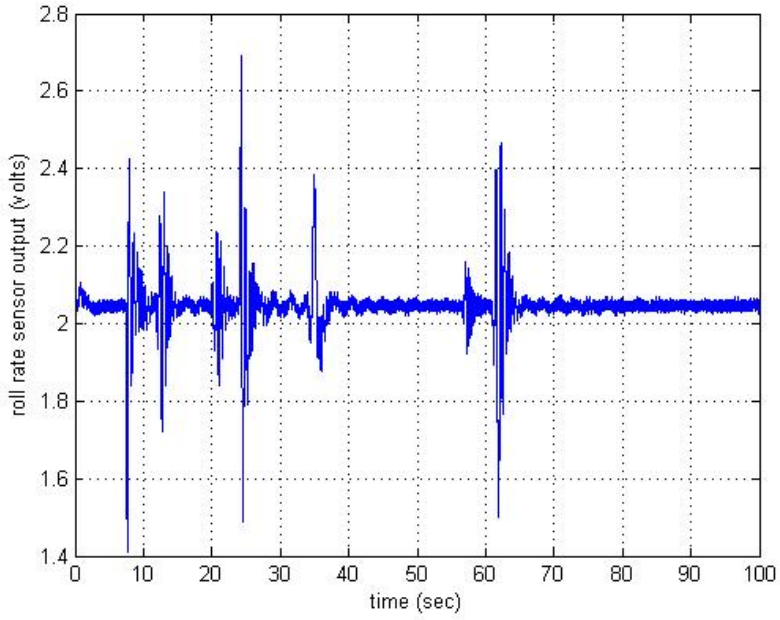

Figure 61 roll rate unfiltered (only factory-set filter on the sensor) sensor output

Use of unshielded cables for signal transmission to the data acquisition card also created noise problems in the system. In order to prevent this noise all of the signal transmitting cables are replaced with a 1mm shielded cable and the shields of the

cables are connected to the ground of the sensors [40]. As a result, signals are shielded and the spikes (Figure 62) in the signals are disappeared.

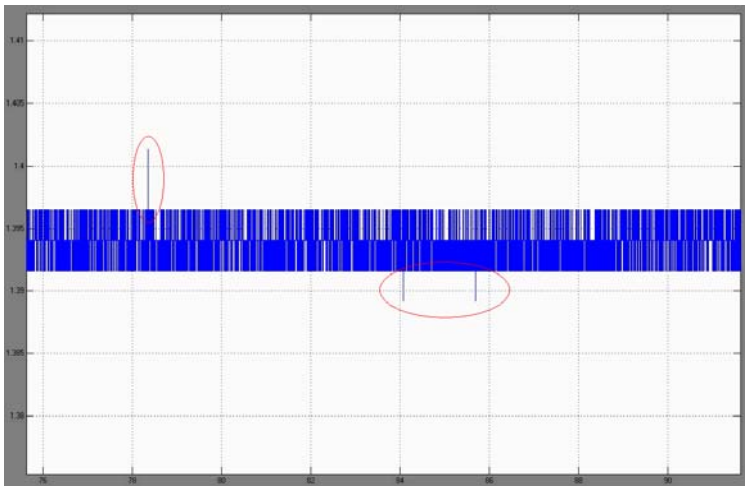

Figure 62 Three spikes in the accelerometer signal (one at the top and two at the bottom)

Also all outputs of the sensors are connected to the data acquisition card through 10 kΩ resistors and ground coupled 0.1 μF capacitors in order to reduce the order of magnitude of the spike noise inherent in the signal outputs by lowpass filtering [40].

Three basic types of noise are mentioned in the literature [41]. Namely they are transmitted, intrinsic and inductive noise. The first type of noise is the one coming in the original signal which is therefore hard to separate from the original signal. The second type is the intrinsic type of noise that is created by the surrounding electronic circuitry. And the final type of noise is inductive one which is caused by the electric fields around. A.M. signals in the air also create this type of noise [40].

The inductive noise problem avoided using shielded cables. But the experiments showed that the main source of the noise problem is the motors which are driven with PWM signals. The fast changes in the signal voltage level, creates strong electromagnetic and pure magnetic fields which highly affect any small signal in the system.

The power sources that are digitally regulated also creates noise [41] therefore, 12 V rechargeable battery is used to supply the sensor set. As a result the noise problem substantially decreased but could not be avoided completely.

After the sensor outputs are filtered and the signal cables are shielded the system was given a disturbance and the controller rapidly responded and rejected the disturbance as shown in the Figures 54-56. The disturbance given to the system is created by turning the quadrotor frame around pitch, roll, and yaw angles respectively.

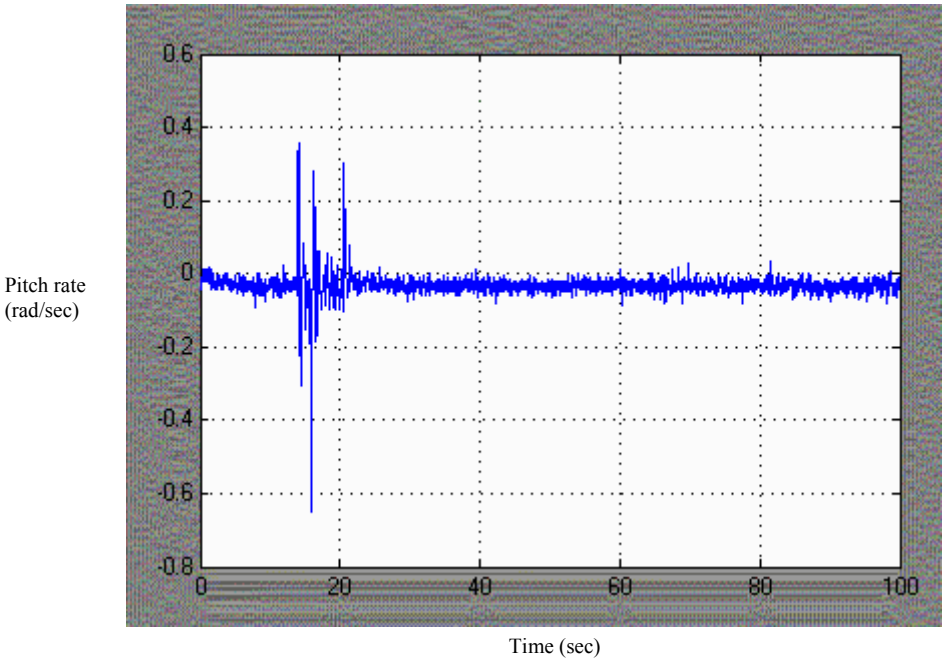

Figure 63 LQR control of pitch rate with a disturbance

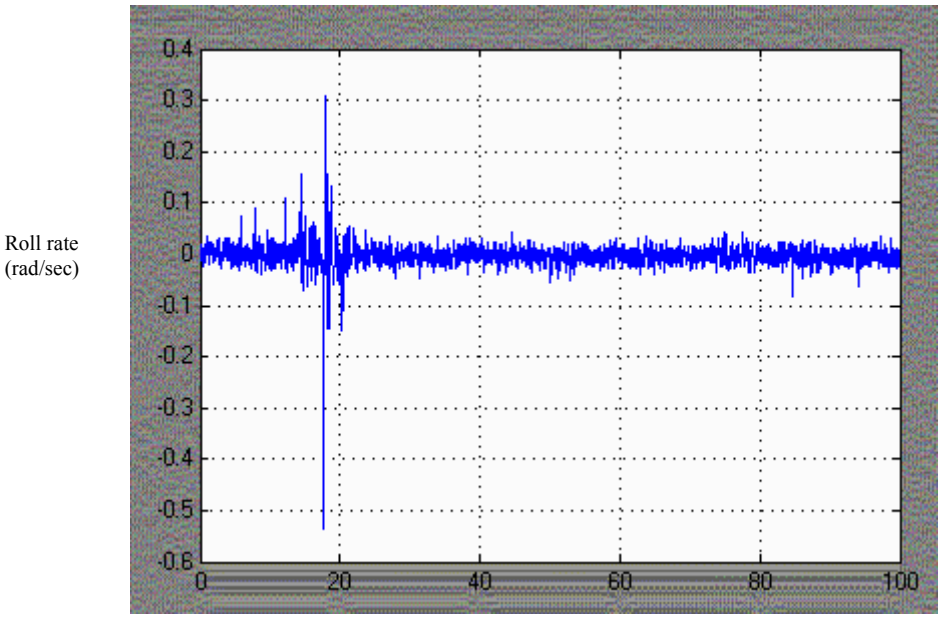

Figure 64 LQR control of roll rate with a disturbance

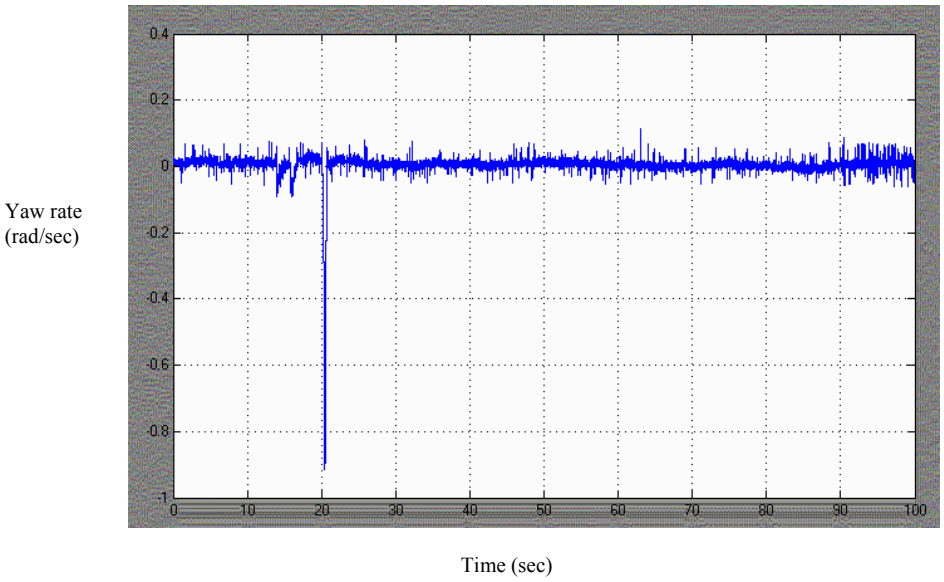

Figure 65 LQR control of yaw rate with a disturbance

CHAPTER 8

DISCUSSIONS AND CONCLUSIONS

In this study the DraganFlyer Vti Quadrotor is used as a test bed for the implementation. Nonlinear state equations for the Quadrotor system have been derived. Then these nonlinear equations have been linearized around the hovering state conditions. The controllability and observability matrices have been investigated for the sensor set. It is seen that the system at hand is fully controllable and attitude dynamics completely observable with the utilized sensor set combinations.

As a result of this study a quadrotor with a carbon fiber body frame has been assembled and real time implementation of a LQR control for the attitude stabilization has been done and shown to work with the hardware setup at sub hovering conditions. Six states are measured with the sensor set consisting of three ADXRS150 gyros, one HMC2003 three axes magnetometer and an ADXL203 two axis accelerometer.

The Magnetometers are highly sensitive to the electromagnetic and pure magnetic fields. Especially the electromagnetic fields produced by the motors and their power cables affect the output of these sensors. It is seen in the experiments that the radiation from the nearby cellular phones has distorted the sensor's output.

The Magnetic field caused by the power cables changes at the same frequency with the PWM motor signals. So an 8^{th} order 20 Hz low-pass Butterworth filter placed at the sensor output, has canceled the noise that is around this PWM frequency (232.6Hz). So driving the motors with a PWM signal seems to be advantageous. In addition to these precautions the magnetometer has been placed as far as possible to the power cables.

The system setup is hanged from the ceiling with a rope. The rope is attached to the frame as close as possible to the center of gravity. Therefore moments due to the rope on the frame are also reduced.

The cables connecting the sensor and onboard driver set to the computer have created a problem on the system. The bundled cables have resulted in a relatively stiff connection and affected the system performance. During the side sways and near the hovering condition the cables have moved and changed both the center of gravity and the mass of the overall system. The bundling of the cables has reduced this effect but could not cancel it.

The unbalanced propellers have caused excessive vibrations which increased the noise in the accelerometer outputs. Part of this noise due to vibration has been reduced using lowpass 8^{th} order Butterworth filters but couldn't be canceled totally. Other than the vibrations there are also accelerations because of the motion of the quadrotor. These motions are sensed by the accelerometers. This generates errors in the roll and pitch angle measurements. In order to improve the accuracy of euler angle measurements, state estimation can be employed.

The real system is assembled and tested. And finally the LQR control method is implemented to work in real time. The attitude of the system is stabilized at sub hovering condition but the system has shown a poor performance at the hovering state. Near hovering the system is tilted to one side. There are several reasons which can lead to this problem. Firstly, the motors are represented with a linear approximation in the model which is not a very accurate but simple assumption. Dynamic models of the motors could be derived and used instead of linearized approximations. Secondly, the LQR controller can be tuned for better performance. Finally, the signal wires can be replaced with thinner wires to eliminate the stiffness due to the present cables.

REFERENCES

[1] J.G.Leisman, Evolution of Helicopter Flight, http:// www.100yearsofflight.com, retrieved December 2006.

[2] Bell/Boeing-Vertol v-22Osprey, 1989, http://avia.russian.ee/vertigo/tiltrotor.html retrieved December 2006.

[3] E.N.Johnson, UAV research at Georgia tech., Georgia Tech School of Aerospace Engineering, June 3, 2002, http://www.ae.gatech.edu/, retrieved December 2006

[4] M. Chen, M. Huzmezan, A Combined MBPC/ 2 DOF H∞ Controller for a Quad Rotor UAV, Department of Electrical and Computer Engineering University of British Columbia Vancouver, BC, Canada, V6T 1Z4, 2003.

[5] S.K.Hong, Fuzzy logic based closed-loop strap down attitude system for unmanned aerial vehicle (UAV), Department of Aerospace Engineering, Sejong University, 2005.

[6] E.Altuğ, Vision based control of unmanned aerial vehicles with applications to an autonomous four rotor helicopter, Quadrotor, PhD thesis, University of Pennsylvania, 2003.

[7] J. S. Jang, Nonlinear control using discrete-time dynamic inversion under input saturation theory and experiment on the Stanford dragon fly UAVS., PhD thesis, Stanford University, 2003.

[8] P. Castillo, A. Dzul and R. Lozano, Real-time Stabilization and Tracking of a Four Rotor Mini-Rotorcraft, submitted to IEEE transactions on control systems technology,2003.

[9] L. Klauske, T. Lorenz, N. Colberg, M. Janke, U. Monich, N. Nothing, L. Thiele, F. Venzke, T. Wernicke S. Zeiler and R. Kusch , DSP-Copter - A Quadrotor Helicopter Controlled by a Digital Signal Processor , ELITE-Project Report Summary, 2002.

[10] E. B. Nice, Design of a Four Rotor Hovering Vehicle, M.S. thesis, Cornell University, 2003.

[11] B. Pongpaibul, Experimental Flying Autonomous Vehicle, MEng Cybernetics, 2001.

[12] R. Siegwart, D. Burnier, J.-C. Zufferey, Computer-Based Control System for a Model Helicopter, Microengineering Department Semester Project Report, 2002.

[13] S. Bouabdallah, P. Murrieri, R. Siegwart, Design and Control of an Indoor Micro Quadrotor, 2002.

[14] P.Pounds , R.Mahony, P. Hynes, J. Roberts, Design of a four-rotor aerial robot, Australiasian Conference on Robotics and Automation Auckland, 27-29 November 2002.

[15] Wikipedia the free encyclopedia, http//en.wikipedia.org/wiki/Main_Page, retrieved December 2006.

[16] A.D.King, Inertial Navigation Forty Years of Evolution, Marconi Electronic systems Ltd., www.imar-navigation.de, retrieved august 2006.

[17] Ari Y.Benbasat, Joseph A.Paradiso, An Inertial Measurement Framework for Gesture Recognition and Applications, MIT Media Laboratory, 2005.

[18] Integrated Inertial Positioning Systems, Zupt, LLC, http://www.imar-navigation.de/englishside/downl_engl/workengl.htm, retrieved December 2006.

[19] R. Siegwart, Synthèse et Implémentation d'un Contrôleur pour Micro Hélicoptère à 4 Rotors, institut d'ingenierie des systemes, i2s Autonomous systems lab, asl, February 2004.

[20] M.I. Ribeiro, Kalman and Extended Kalman Filters: Concept, Derivation and Properties, Instituto Superior Tcnico Av. Rovisco Pais Lisboa, Portugal, February 2004, retrieved December 2006.

[21] W. Greg, B. Gary, An introduction to the Kalman Filter, Department of Computer Science, University of North Carolina at Chapel Hill, http://www.cs.unc.edu/~{welch,gb}, retrieved December 2001

[22] MATLAB documentation, www.mathworks.com, retrieved December 2006.

[23] RC toys web site, www.rctoys.com., retrieved December 2006.

[24] Honeywell documentation, www.honeywell.com, retrieved December 2006.

[25] Memsic Documentation, www.memsic.com, retrieved December 2006.

[26] Silicon Sensing Documentation, www.siliconsensing.com, retrieved December 2006.

[27] Analog devices Documentation, www.analog.com, retrieved December 2006.

[28] Parallax Documentation, www.parallaxinc.com, retrieved December 2006.

[29] humusoft Mf 614 data acquisition card, http://www.humusoft.cz/datacq/mf614.htm, retrieved December 2006.

[30]Sandia National Laboratories, SUMMiTTM Technologies, www.mems.sandia.gov, retrieved December 2006.

[31] K.Ogata, Modern Control Engineering, forth edition, Prentice Hall, pg 781-786 , 2002.

[32] B.Çamlıca, Demonstration of a stabilized hovering platform for undergraduate laboratory, December 2004.

[33] Floyd, Electronic Devices, third edition, Merrill, 1992.

[34] International rectifier, IRFZ44N & IRLZ44N mosfet transistors' datasheet. www.irf.com, retrieved December 2006

[35] Scott D. Hanford, A Small Semi-Autonomous Rotary-Wing Unmanned Air Vehicle (UAV), Master thesis, December 2005.

[36] www.astroflight.com, 204D speed controller datasheet, retrieved December 2006

[37] http://solutions-cubed.com/Solutions%20Cubed/index.htm, simple H bridge datasheet, retrieved December 2006

[38] www.microchip.com, 16F877 datasheet, retrieved December 2006

[39] http://www.epanorama.net/links/motorcontrol.html, retrieved December 2006

[40] P.Klonowski, Use of the AD590 Temperature Transducer in a Remote Sensing Application, analog devices inc., www.analog.com, retrieved December 2006.

[41] A.Rich, Shielding and Guarding, analog devices, www.analog.com, retrieved December 2006.

[42] ADXL203EB datasheet, www.analog.com, retrieved December 2006.

[43] S.Sassen, P. Uhleman, Quattrocopter A unique Micro-Aerial Vehicle, European Aeronautic Defense and Space Company Corporate research centre, November 2003.

[44] P.Pounds , R.Mahony, J.Gresham, Towards Dynamically-Favourable Quad-Rotor Aerial Robots, Australian National University, Canberra, Australia, 2004.

[45] G.Hoffmann, D.Dostal, S.Waslander, J.Jang, C.Tomlin, Stanford Testbed of Autonomous Rotorcraft for Multi-Agent Control(STARMAC), Stanford university, October 28th, 2004.

APPENDICES

APPENDIX 1

CONTROLLABILITY AND OBSERVABILTY MATRIX

The Controllability Matrix:

```
Colums 1 to 12
0       0       0       0       0       0       0       0       0       0       0       0
0       0       0       0       0       0       0       0       0       0       0       0
0       0       0       0       -1.00   -1.00   -1.00   -1.00   0       0       0       0
0       0       0       0       0       0       0       0       9.81    0       -9.81   0
0       0       0       0       0       0       0       0       9.81    9.81    9.81    9.81
1.00    1.00    1.00    1.00    0       0       0       0       0       0       0       0
-1.00   0       1.00    0       0       0       0       0       0       0       0       0
0       -1.00   0       1.00    0       0       0       0       0       0       0       0
1.00    1.00    1.00    1.00    0       0       0       0       0       0       0       0
0       0       0       0       -1.00   0       1.00    0       0       0       0       0
0       0       0       0       0       -1.00   0       1.00    0       0       0       0
0       0       0       0       1.00    1.00    1.00    1.00    0       0       0       0

Colums 13 to 24
9.81    0       -9.81   0       0       0       0       0       0       0       0       0
19.62   9.81    0       9.81    0       0       0       0       0       0       0       0
0       0       0       0       0       0       0       0       0       0       0       0
0       0       0       0       0       0       0       0       0       0       0       0
0       0       0       0       0       0       0       0       0       0       0       0
0       0       0       0       0       0       0       0       0       0       0       0
0       0       0       0       0       0       0       0       0       0       0       0
0       0       0       0       0       0       0       0       0       0       0       0
0       0       0       0       0       0       0       0       0       0       0       0
0       0       0       0       0       0       0       0       0       0       0       0
0       0       0       0       0       0       0       0       0       0       0       0
0       0       0       0       0       0       0       0       0       0       0       0
```

all columns between 25 to 48 is zero.

The rank of the controllability matrix is 12 which means that the system is completely state controllable.

The Observability Matrix:

The rank of the observability matrix given below is six. This states the complete observability of the system.

$$
\begin{bmatrix}
1 & 0 & 0 & 0 & 0 & 0 \\
0 & 1 & 0 & 0 & 0 & 0 \\
0 & 0 & 1 & 0 & 0 & 0 \\
0 & 0 & 0 & 1 & 0 & 0 \\
0 & 0 & 0 & 0 & 1 & 0 \\
0 & 0 & 0 & 0 & 0 & 1 \\
0 & 0 & 0 & 0 & 0 & 0 \\
0 & 0 & 0 & 0 & 0 & 0 \\
0 & 0 & 0 & 0 & 0 & 0 \\
1.0000 & 0 & 0 & 0 & 0 & 0 \\
0 & 0.9950 & -0.0998 & 0 & 0 & 0 \\
0 & 0.0998 & 0.9950 & 0 & 0 & 0 \\
0 & 0 & 0 & 0 & 0 & 0 \\
0 & 0 & 0 & 0 & 0 & 0 \\
0 & 0 & 0 & 0 & 0 & 0 \\
0 & 0 & 0 & 0 & 0 & 0 \\
0 & 0 & 0 & 0 & 0 & 0 \\
0 & 0 & 0 & 0 & 0 & 0 \\
0 & 0 & 0 & 0 & 0 & 0 \\
0 & 0 & 0 & 0 & 0 & 0 \\
0 & 0 & 0 & 0 & 0 & 0 \\
0 & 0 & 0 & 0 & 0 & 0 \\
0 & 0 & 0 & 0 & 0 & 0 \\
0 & 0 & 0 & 0 & 0 & 0 \\
0 & 0 & 0 & 0 & 0 & 0 \\
0 & 0 & 0 & 0 & 0 & 0 \\
0 & 0 & 0 & 0 & 0 & 0 \\
0 & 0 & 0 & 0 & 0 & 0 \\
0 & 0 & 0 & 0 & 0 & 0 \\
0 & 0 & 0 & 0 & 0 & 0 \\
0 & 0 & 0 & 0 & 0 & 0 \\
0 & 0 & 0 & 0 & 0 & 0 \\
0 & 0 & 0 & 0 & 0 & 0
\end{bmatrix}
$$

0 0 0 0 0 0
0 0 0 0 0 0
0 0 0 0 0 0

APPENDIX 2

MOTOR DATASHEET

MABUCHI MOTORS DATASHEET

Draganflyer Vti model utilizes four Mabuchi motors the data of which is given in the following spec sheet. [23]

Table 4 Mabuchi motor specs.

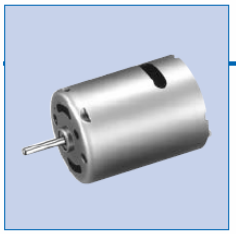

RK-370SD

MABUCHI MOTOR
Carbon-brush motors

OUTPUT : 0.5W~24W (APPROX)

WEIGHT : 51g (APPROX)

Typical Applications **Toys and Models :** Radio Control Model

MODEL	VOLTAGE		NO LOAD		AT MAXIMUM EFFICIENCY					STALL		
	OPERATING RANGE	NOMINAL	SPEED	CURRENT	SPEED	CURRENT	TORQUE		OUTPUT	TORQUE		CURRENT
			r/min	A	r/min	A	mN·m	g·cm	W	mN·m	g·cm	A
RK-370SD-2870 (*1)	4.5~9.6	7.2V CONSTANT	16500	0.34	13790	1.73	5.97	60.9	8.61	36.3	370	8.77

(*1) CCW shifted commutation (CCW+)
The terminal position against the tapped holes varies depending on CW+/NEUTRAL.

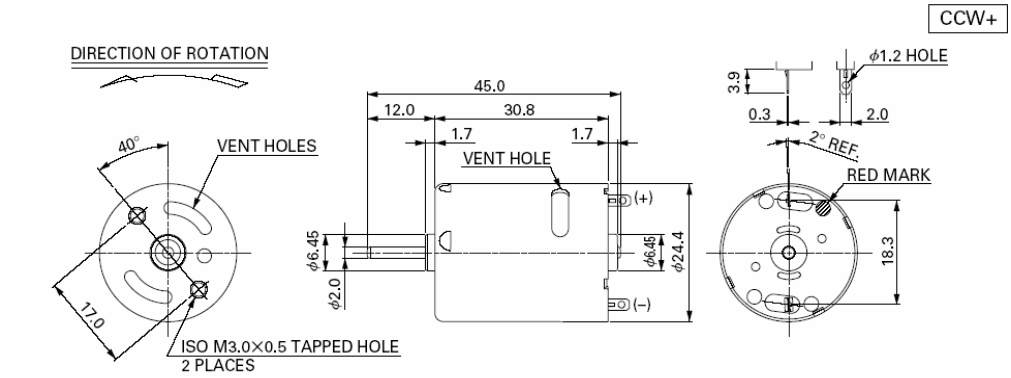

Usable machine screw length 2.0 max. from motor mounting surface.

UNIT: MILLIMETERS

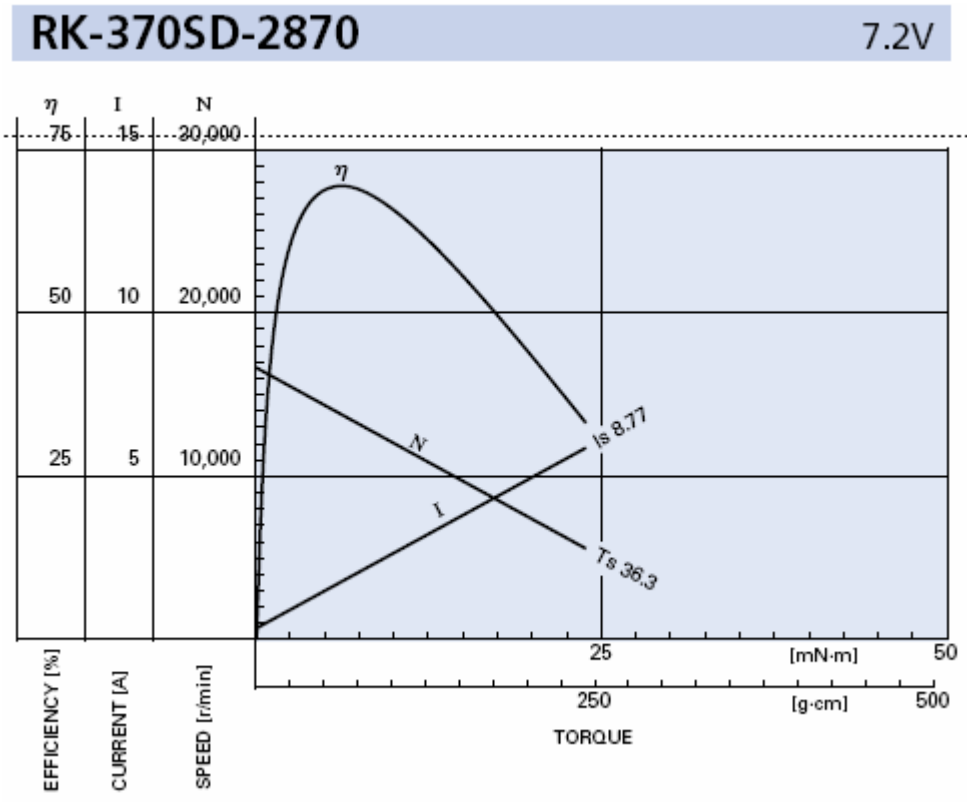

Table 5 IRFZ44N specs.

Electrical Characteristics @ T_J = 25°C (unless otherwise specified)

	Parameter	Min.	Typ.	Max.	Units	Conditions
$V_{(BR)DSS}$	Drain-to-Source Breakdown Voltage	55	—	—	V	V_{GS} = 0V, I_D = 250µA
$\Delta V_{(BR)DSS}/\Delta T_J$	Breakdown Voltage Temp. Coefficient	—	0.055	—	V/°C	Reference to 25°C, I_D = 1mA
$R_{DS(on)}$	Static Drain-to-Source On-Resistance	—	—	0.022	Ω	V_{GS} = 10V, I_D = 25A ④
$V_{GS(th)}$	Gate Threshold Voltage	2.0	—	4.0	V	V_{DS} = V_{GS}, I_D = 250µA
g_{fs}	Forward Transconductance	17	—	—	S	V_{DS} = 25V, I_D = 25A
I_{DSS}	Drain-to-Source Leakage Current	—	—	25	µA	V_{DS} = 55V, V_{GS} = 0V
		—	—	250		V_{DS} = 44V, V_{GS} = 0V, T_J = 150°C
I_{GSS}	Gate-to-Source Forward Leakage	—	—	100	nA	V_{GS} = 20V
	Gate-to-Source Reverse Leakage	—	—	-100		V_{GS} = -20V
Q_g	Total Gate Charge	—	—	65	nC	I_D = 25A
Q_{gs}	Gate-to-Source Charge	—	—	12		V_{DS} = 44V
Q_{gd}	Gate-to-Drain ("Miller") Charge	—	—	27		V_{GS} = 10V, See Fig. 6 and 13 ④
$t_{d(on)}$	Turn-On Delay Time	—	7.3	—	ns	V_{DD} = 28V
t_r	Rise Time	—	69	—		I_D = 25A
$t_{d(off)}$	Turn-Off Delay Time	—	47	—		R_G = 12Ω
t_f	Fall Time	—	60	—		R_D = 1.1Ω, See Fig. 10 ④
L_D	Internal Drain Inductance	—	4.5	—	nH	Between lead, 6mm (0.25in.) from package and center of die contact
L_S	Internal Source Inductance	—	7.5	—		
C_{iss}	Input Capacitance	—	1300	—	pF	V_{GS} = 0V
C_{oss}	Output Capacitance	—	410	—		V_{DS} = 25V
C_{rss}	Reverse Transfer Capacitance	—	150	—		f = 1.0MHz, See Fig. 5

APPENDIX 3

SENSOR DATASHEETS

ANALOG DEVICES

±150°/s Single Chip Yaw Rate Gyro with Signal Conditioning

ADXRS150

FEATURES

- Complete rate gyroscope on a single chip
- Z-axis (yaw rate) response
- High vibration rejection over wide frequency
- 0.05°/s/√Hz noise
- 2000 *g* powered shock survivability
- Self-test on digital command
- Temperature sensor output
- Precision voltage reference output
- Absolute rate output for precision applications
- 5 V single-supply operation
- Ultrasmall and light (< 0.15 cc, < 0.5 gram)

APPLICATIONS

- GPS navigation systems
- Vehicle stability control
- Inertial measurement units
- Guidance and control
- Platform stabilization

GENERAL DESCRIPTION

The ADXRS150 is a complete angular rate sensor (gyroscope) that uses Analog Devices' surface-micromachining process to make a functionally complete and low cost angular rate sensor integrated with all of the required electronics on one chip.

The manufacturing technique for this device is the same high volume BIMOS process used for high reliability automotive airbag accelerometers.

The output signal, RATEOUT (1B, 2A), is a voltage proportional to the angular rate about the axis normal to the top surface of the package (see Figure 2). A single external resistor can be used to lower the scale factor. An external capacitor is used to set the bandwidth. Other external capacitors are required for operation (see Figure 22).

A precision reference and a temperature output are also provided for compensation techniques. Two digital self-test inputs electromechanically excite the sensor to test the operation of both sensors and the signal conditioning circuits. The ADXRS150 is available in a 7 mm × 7 mm × 3 mm BGA surface-mount package.

FUNCTIONAL BLOCK DIAGRAM

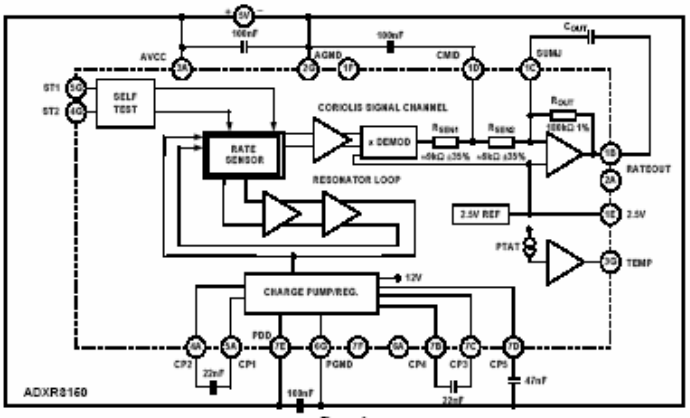

Figure 1.

One Technology Way, P.O. Box 9106, Norwood, MA 02062-9106, U.S.A.
Tel: 781.329.4700 www.analog.com
Fax: 781.326.8703

SPECIFICATIONS

@T_A = 25°C, V_S = 5 V, bandwidth = 80 Hz (C_{OUT} = 0.01 µF), angular rate = 0°/s, ±1g, unless otherwise noted.

Table 1.

Parameter	Conditions	ADXRS150ABG			Unit
		Min[1]	Typ	Max[1]	
SENSITIVITY	Clockwise rotation is positive output				
Dynamic Range[2]	Full-scale range over specifications range	±150			°/s
Initial	@25°C	11.25	12.5	13.75	mV/°/s
Over Temperature[3]	V_{CC} = 4.75 V to 5.25 V	11.25		13.75	mV/°/s
Nonlinearity	Best fit straight line		0.1		% of FS
Voltage Sensitivity	V_{CC} = 4.75 V to 5.25 V		0.7		%/V
NULL					
Initial Null			2.50		V
Null Drift over Temperature[3]	Delta from 25°C			±300	mV
Turn-On Time	Power on to ±½°/s of final		35		ms
Linear Acceleration Effect	Any axis		0.2		°/s/*g*
Voltage Sensitivity	V_{CC} = 4.75 V to 5.25 V		1		°/s/V
NOISE PERFORMANCE					
Rate Noise Density	@25°C		0.05		°/s/√Hz
FREQUENCY RESPONSE					
3 db Bandwidth[4] (User Selectable)	22 nF as comp cap (see the Applications section)		40		Hz
Sensor Resonant Frequency			14		kHz
SELF TEST					
ST1 RATEOUT Response[5]	ST1 pin from Logic 0 to 1, –40°C to +85°C	–400	–660	–1000	mV
ST2 RATEOUT Response[5]	ST2 pin from Logic 0 to 1, –40°C to +85°C	+400	+660	+1000	mV
Logic 1 Input Voltage	Standard high logic level definition	3.3			V
Logic 0 Input Voltage	Standard low logic level definition			1.7	V
Input Impedance	To common		50		kΩ
TEMPERATURE SENSOR					
V_{OUT} at 298°K			2.50		V
Max Current Load on Pin	Source to common			50	µA
Scale Factor	Proportional to absolute temperature		8.4		mV/°K
OUTPUT DRIVE CAPABILITY					
Output Voltage Swing	I_{OUT} = ±100 µA	0.25		V_S – 0.25	V
Capacitive Load Drive		1000			pF
2.5 V REFERENCE					
Voltage Value		2.45	2.5	2.55	V
Load Drive to Ground	Source		200		µA
Load Regulation	0 < I_{OUT} < 200 µA		5.0		mV/mA
Power Supply Rejection	4.75 V_S to 5.25 V_S		1.0		mV/V
Temperature Drift[3]	Delta from 25°C		5.0		mV
POWER SUPPLY					
Operating Voltage Range		4.75	5.00	5.25	V
Quiescent Supply Current			6.0	8.0	mA
TEMPERATURE RANGE					
Specified Performance Grade A		–40		+85	°C

[1] All min and max specifications are guaranteed. Typical specifications are not tested or guaranteed.
[2] Dynamic range is the maximum full-scale measurement range possible, including output swing range, initial offset, sensitivity, offset drift, and sensitivity drift at 5 V supplies.
[3] Specification refers to the maximum extent of this parameter as a worst-case value at T_{MIN} or T_{MAX}.
[4] Frequency at which response is 3 dB down from dc response with specified compensation capacitor value. Internal pole forming resistor is 180 kΩ. See the Setting Bandwidth section.
[5] Self-test response varies with temperature. See the Self-Test Function section for details.

ABSOLUTE MAXIMUM RATINGS

Table 2.

Parameter	Rating
Acceleration (Any Axis, Unpowered, 0.5 ms)	2000 *g*
Acceleration (Any Axis, Powered, 0.5 ms)	2000 *g*
$+V_S$	−0.3 V to +6.0 V
Output Short-Circuit Duration (Any Pin to Common)	Indefininte
Operating Temperature Range	−55°C to +125°C
Storage Temperature	−65°C to +150°C

Stresses above those listed under Absolute Maximum Ratings may cause permanent damage to the device. This is a stress rating only and functional operation of the device at these or any other conditions above those indicated in the operational section of this specification is not implied. Exposure to absolute maximum rating conditions for extended periods may affect device reliability.

Applications requiring more than 200 cycles to MIL-STD-883 Method 1010 Condition B (−55°C to +125°C) require underfill or other means to achieve this requirement.

Drops onto hard surfaces can cause shocks of greater than 2000 *g* and exceed the absolute maximum rating of the device. Care should be exercised in handling to avoid damage.

RATE SENSITIVE AXIS

This is a Z-axis rate-sensing device that is also called a yaw rate sensing device. It produces a positive going output voltage for clockwise rotation about the axis normal to the package top, i.e., clockwise when looking down at the package lid.

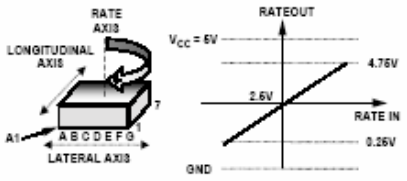

Figure 2. RATEOUT Signal Increases with Clockwise Rotation

ESD CAUTION

ESD (electrostatic discharge) sensitive device. Electrostatic charges as high as 4000 V readily accumulate on the human body and test equipment and can discharge without detection. Although this product features proprietary ESD protection circuitry, permanent damage may occur on devices subjected to high energy electrostatic discharges. Therefore, proper ESD precautions are recommended to avoid performance degradation or loss of functionality.

PIN CONFIGURATION AND FUNCTION DESCRIPTIONS

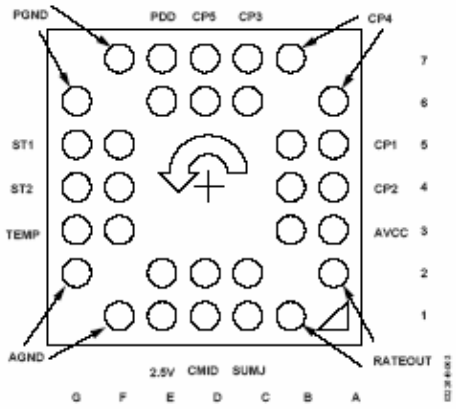

Figure 3. BGA-32 (Bottom View)

Table 3. Pin Function Descriptions

Pin No.	Mnemonic	Description
6D, 7D	CP5	HV Filter Capacitor—47 nF
6A, 7B	CP4	Charge Pump Capacitor—22 nF
6C, 7C	CP3	Charge Pump Capacitor—22 nF
5A, 5B	CP1	Charge Pump Capacitor—22 nF
4A, 4B	CP2	Charge Pump Capacitor—22 nF
3A, 3B	AVCC	+ Analog Supply
1B, 2A	RATEOUT	Rate Signal Output
1C, 2C	SUMJ	Output Amp Summing Junction
1D, 2D	CMID	HF Filter Capacitor—100 nF
1E, 2E	2.5V	2.5 V Precision Reference
1F, 2G	AGND	Analog Supply Return
3F, 3G	TEMP	Temperature Voltage Output
4F, 4G	ST2	Self-Test for Sensor 2
5F, 5G	ST1	Self-Test for Sensor 1
6G, 7F	PGND	Charge Pump Supply Return
6E, 7E	PDD	+ Charge Pump Supply

±150°/s Single Chip Rate Gyro Evaluation Board

ADXRS150EB

GENERAL DESCRIPTION

The ADXRS150EB is a simple evaluation board that allows the user to quickly evaluate the performance of the ADXRS150ABG yaw rate gyro. No additional external components are required for operation. The ADXRS150EB has a 20-lead dual-in-line (0.3 inch width by 0.1 inch pin spacing) interface that allows the user to easily prototype products without having to deal with BGA soldering. The 0.4 square inch outline of the ADXRS150EB is still among the smallest gyros available today.

CIRCUIT DESCRIPTION

The schematic of the ADXRS150EB is shown in Figure 1. It is identical to the suggested application shown in the ADXRS150ABG data sheet.

The analog and power grounds (AGND and PGND) have separate ground planes and are joined at one point. The user may cut this trace if separate ground schemes are desired.

Note that the analog supply voltage and charge pump supply voltage (AVCC and PDD) are not connected on the ADXRS150EB and that users must connect these as appropriate to their application.

The parts layout of the ADXRS150EB is shown in Figure 2, and the parts list for the ADXRS150EB is shown in Table I. As delivered, the ADXRS150EB is set for 40 Hz bandwidth (C_{OUT} = 22 nF). The user may add an external capacitor to further reduce the bandwidth and improve the noise floor.

SPECIAL NOTES ON HANDLING

Note that the ADXRS150EB is not reverse polarity protected. Reversing the power supply or applying inappropriate voltages to any pin (outside the data sheet's Absolute Maximum Ratings) may damage the ADXRS150EB.

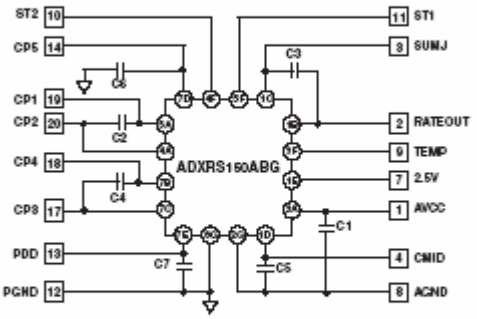

Figure 1. ADXRS150EB Schematic

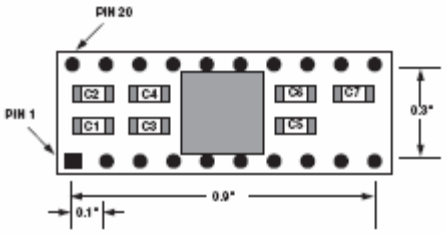

Figure 2. ADXRS150EB Parts Layout

Table I. ADXRS150EB Parts List

Component	Value (nF)
C1	100
C2	22
C3	22
C4	22
C5	100
C6	47
C7	100

REV. 0

One Technology Way, P.O. Box 9106, Norwood, MA 02062-9106, U.S.A.
Tel: 781/329-4700 www.analog.com
Fax: 781/326-8703

THREE-AXIS MAGNETIC SENSOR HYBRID

Features

- 20-pin Wide DIP Footprint (1" by 0.75")
- Precision 3-axis Capability
- Factory Calibrated Analog Outputs
- 40 micro-gauss to ±2 gauss Dynamic Range
- Analog Output at 1 Volt/gauss (2.5V @ 0 gauss)
- Onboard +2.5 Volt Reference
- +6 to +15 Volt DC Single Supply Operation
- Very Low Magnetic Material Content
- -40° to 85°C Operating Temperature Range

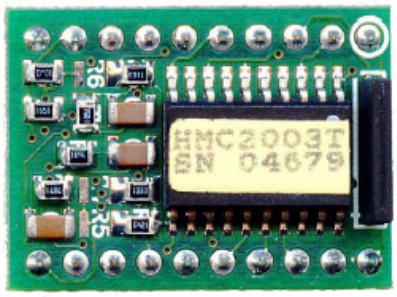

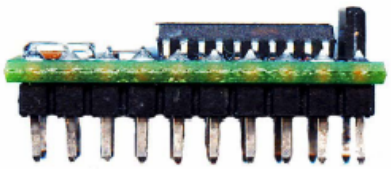

General Description

The Honeywell HMC2003 is a high sensitivity, three-axis magnetic sensor hybrid assembly used to measure low magnetic field strengths. Honeywell's most sensitive magneto-resistive sensors (HMC1001 and HMC1002) are utilized to provide the reliability and precision of this magnetometer design. The HMC2003 interface is all analog with critical nodes brought out to the pin interfaces for maximum user flexibility. The internal excitation current source and selected gain and offset resistors, reduces temperature errors plus gain and offset drift. Three precision low-noise instrumentation amplifiers with 1kHz low pass filters provide accurate measurements while rejecting unwanted noise.

APPLICATIONS

- Precision Compassing
- Navigation Systems
- Attitude Reference
- Traffic Detection
- Proximity Detection
- Medical Devices

BLOCK DIAGRAM

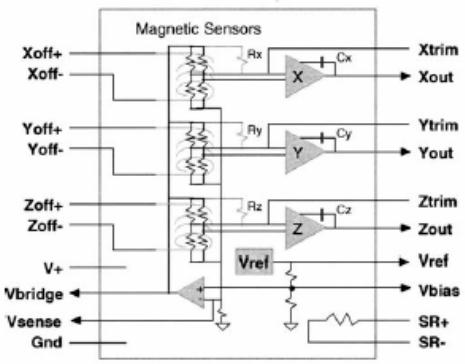

SPECIFICATIONS

Characteristics	Conditions[1]	Min	Typ	Max	Units[2]
Magnetic Field					
Sensitivity		0.98	1	1.02	V/gauss
Null Field Output		2.3	2.5	2.7	V
Resolution			40		μgauss
Field Range	Maximum Magnetic Flux Density	-2		2	gauss
Output Voltage	Each Magnetometer Axis Output	0.5		4.5	
Bandwidth			1		kHz
Errors					
Linearity Error	±1 gauss Applied Field Sweep ±2 gauss Applied Field Sweep		0.5 1	2 2	%FS
Hysteresis Error	3 Sweeps across ±2 gauss		0.05	0.1	%FS
Repeatability Error	3 Sweeps across ±2 gauss		0.05	0.1	%FS
Power Supply Effect	PS Varied from 6 to 15V With ±1 gauss Applied Field Sweep			0.1	%FS
Offset Strap					
Resistance				10.5	ohms
Sensitivity		46.5	47.5	48.5	mA/gauss
Current				200	mA
Set/Reset Strap					
Resistance			4.5	6	ohms
Current	2msec pulse, 1% duty cycle	3.0	3.2	5	amps
Tempcos					
Field Sensitivity			-600		ppm/°C
Null Field	Set/Reset Not Used Set/Reset Used		±400 ±100		ppm/°C
Environments					
Temperature	Operating Storage	-40 -55	- -	+85 +125	°C °C
Shock			100		g
Vibration			2.2		g rms
Electrical					
Supply Voltage[3]		6		15	VDC
Supply Current				20	mA

(1) Unless otherwise stated, test conditions are as follows: Power Supply = 12VDC, Ambient Temp = 25°C, Set/Reset switching is active

(2) Units: 1 gauss = 1 Oersted (in air) = 79.58 A/m = 10E5 gamma

(3) Transient protection circuitry should be added across V+ and Gnd if an unregulated power supply is used.

General Description

Honeywell's three axis magnetic sensor hybrid uses three permalloy magneto-resistive sensors and custom interface electronics to measure the strength and direction of an incident magnetic field. These sensors are sensitive to magnetic fields along the length, width, and height (X, Y, Z axis) of the 20-pin dual-in-line hybrid. Fields can be detected less than 40 microgauss and up to ±2 gauss. Analog outputs are available for each X, Y and Z axis from the hybrid. With the sensitivity and linearity of this hybrid, changes can be detected in the earth's magnetic field to provide compass headings or attitude sensing. The high bandwidth of this hybrid allows for anomaly detection of vehicles, planes, and other ferrous objects at high speeds.

The hybrid is packaged on a small printed circuit board (1" by 0.75") and has an on-chip +2.5 voltage reference that operates from a single 6 to 15V supply. The hybrid is ideal for applications that require two- or three-axis magnetic sensing and have size constraints and need a magnetic transducer (magnetometer) front-end. Note that the hybrid's resistor values will vary, or an abscense of some resistor components, is likely due to individual factory calibration.

Integrated with the sensor elements composed of wheatstone bridge circuits, are magnetically coupled straps that replace the need for external field coils and provide various modes of operation. The Honeywell patented integrated field offset straps (Xoff+ and Xoff-, etc.) can be used electrically to apply local magnetic fields to the bridges to buck, or offset an applied incident field. This technique can be used to cancel unwanted ambient magnetic fields (e.g. hard-iron magnetism) or in a closed loop field nulling measurement circuit. The offset straps nominally provide 1 gauss fields along the sensitive axis per 48mA of offset current through each strap.

The HMC2003's magnetic sensors can be affected by high momentary magnetic fields that may lead to output signal degradation. In order to eliminate this effect, and maximize the signal output, a magnetic switching technique can be applied to the bridge using set/reset pins (SR+ and SR-) that eliminates the effect of past magnetic history. Refer to the application notes that provide information on set/reset circuits and operation.

Pinout Diagram and Package Drawing

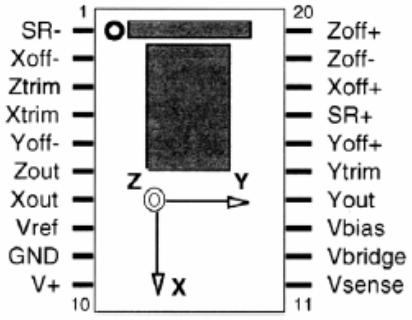

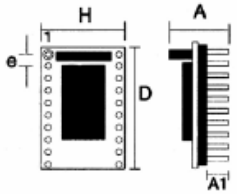

Symbol	Millimeters		Inches	
	Min	Max	Min	Max
A	10.92	11.94	0.43	0.47
A1	2.92	3.42	0.115	0.135
D	25.91	27.30	1.02	1.075
e	2.41	2.67	0.095	0.105
H	18.03	19.69	0.71	0.775

Ordering Information

Ordering Number	Product
HMC2003	Three-Axis Magnetic Sensor Hybrid

Precision ±1.7 *g* Single-/Dual-Axis *i*MEMS® Accelerometer

ADXL103/ADXL203

FEATURES

- High performance, single-/dual-axis accelerometer on a single IC chip
- 5 mm × 5 mm × 2 mm LCC package
- 1 m*g* resolution at 60 Hz
- Low power: 700 µA at V_S = 5 V (typical)
- High zero *g* bias stability
- High sensitivity accuracy
- −40°C to +125°C temperature range
- X and Y axes aligned to within 0.1° (typical)
- BW adjustment with a single capacitor
- Single-supply operation
- 3500 *g* shock survival
- RoHS-compliant
- Compatible with Sn/Pb- and Pb-free solder processes

APPLICATIONS

- Vehicle dynamic control (VDC)/electronic stability program (ESP) systems
- Electronic chassis control
- Electronic braking
- Platform stabilization/leveling
- Navigation
- Alarms and motion detectors
- High accuracy, 2-axis tilt sensing

GENERAL DESCRIPTION

The ADXL103/ADXL203 are high precision, low power, complete single- and dual-axis accelerometers with signal conditioned voltage outputs, all on a single, monolithic IC. The ADXL103/ADXL203 measure acceleration with a full-scale range of ±1.7 *g*. The ADXL103/ADXL203 can measure both dynamic acceleration (for example, vibration) and static acceleration (for example, gravity).

The typical noise floor is 110 µg/√Hz, allowing signals below 1 m*g* (0.06° of inclination) to be resolved in tilt sensing applications using narrow bandwidths (<60 Hz).

The user selects the bandwidth of the accelerometer using Capacitor C_X and Capacitor C_Y at the X_{OUT} and Y_{OUT} pins. Bandwidths of 0.5 Hz to 2.5 kHz may be selected to suit the application.

The ADXL103 and ADXL203 are available in 5 mm × 5 mm × 2 mm, 8-pad hermetic LCC packages.

FUNCTIONAL BLOCK DIAGRAM

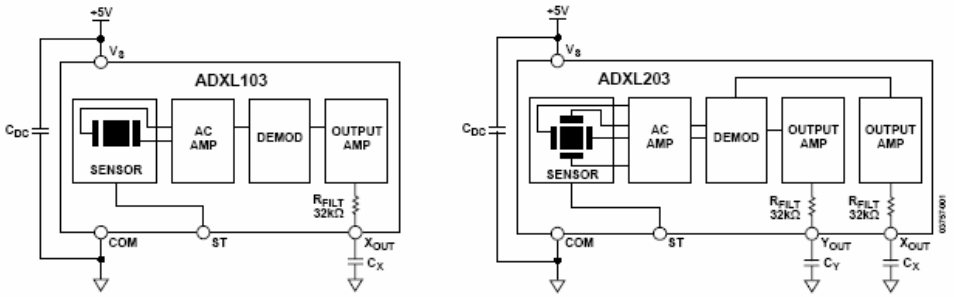

Figure 1.

One Technology Way, P.O. Box 9106, Norwood, MA 02062-9106, U.S.A.
Tel: 781.329.4700 www.analog.com
Fax: 781.461.3113

SPECIFICATIONS

T_A = −40°C to +125°C, V_S = 5 V, C_X = C_Y = 0.1 µF, acceleration = 0 *g*, unless otherwise noted.

Table 1.

Parameter	Conditions	Min[1]	Typ	Max[1]	Unit
SENSOR INPUT	Each axis				
Measurement Range[2]		±1.7			*g*
Nonlinearity	% of full scale		±0.2	±1.25	%
Package Alignment Error			±1		Degrees
Alignment Error (ADXL203)	X sensor to Y sensor		±0.1		Degrees
Cross-Axis Sensitivity			±1.5	±3	%
SENSITIVITY (RATIOMETRIC)[3]	Each axis				
Sensitivity at X_{OUT}, Y_{OUT}	V_S = 5 V	960	1000	1040	mV/*g*
Sensitivity Change Due to Temperature[4]	V_S = 5 V		±0.3		%
ZERO *g* BIAS LEVEL (RATIOMETRIC)	Each axis				
0 *g* Voltage at X_{OUT}, Y_{OUT}	V_S = 5 V	2.4	2.5	2.6	V
Initial 0 *g* Output Deviation from Ideal	V_S = 5 V, 25°C		±25		*mg*
0 *g* Offset vs. Temperature			±0.1	±0.8	*mg*/°C
NOISE PERFORMANCE					
Output Noise	<4 kHz, V_S = 5 V		1	3	mV rms
Noise Density			110		µg/√Hz rms
FREQUENCY RESPONSE[5]					
C_X, C_Y Range[6]		0.002		10	µF
R_{FILT} Tolerance		24	32	40	kΩ
Sensor Resonant Frequency			5.5		kHz
SELF TEST[7]					
Logic Input Low				1	V
Logic Input High		4			V
ST Input Resistance to Ground		30	50		kΩ
Output Change at X_{OUT}, Y_{OUT}	Self Test 0 to Self Test 1	450	750	1100	mV
OUTPUT AMPLIFIER					
Output Swing Low	No load	0.05	0.2		V
Output Swing High	No load		4.5	4.8	V
POWER SUPPLY					
Operating Voltage Range		3		6	V
Quiescent Supply Current			0.7	1.1	mA
Turn-On Time[8]			20		ms

[1] All minimum and maximum specifications are guaranteed. Typical specifications are not guaranteed.
[2] Guaranteed by measurement of initial offset and sensitivity.
[3] Sensitivity is essentially ratiometric to V_S. For V_S = 4.75 V to 5.25 V, sensitivity is 186 mV/V/*g* to 215 mV/V/*g*.
[4] Defined as the output change from ambient-to-maximum temperature or ambient-to-minimum temperature.
[5] Actual frequency response controlled by user-supplied external capacitor (C_X, C_Y).
[6] Bandwidth = 1/(2 × π × 32 kΩ × C). For C_X, C_Y = 0.002 µF, bandwidth = 2500 Hz. For C_X, C_Y = 10 µF, bandwidth = 0.5 Hz. Minimum/maximum values are not tested.
[7] Self-test response changes cubically with V_S.
[8] Larger values of C_X, C_Y increase turn-on time. Turn-on time is approximately 160 × C_X or C_Y + 4 ms, where C_X, C_Y are in µF.

ABSOLUTE MAXIMUM RATINGS

Table 2.

Parameter	Rating
Acceleration (Any Axis, Unpowered)	3500 *g*
Acceleration (Any Axis, Powered)	3500 *g*
Drop Test (Concrete Surface)	1.2 m
V_S	−0.3 V to +7.0 V
All Other Pins	(COM − 0.3 V) to (V_S + 0.3 V)
Output Short-Circuit Duration (Any Pin to Common)	Indefinite
Temperature Range (Powered)	−55°C to +125°C
Temperature Range (Storage)	−65°C to +150°C

Stresses above those listed under Absolute Maximum Ratings may cause permanent damage to the device. This is a stress rating only; functional operation of the device at these or any other conditions above those indicated in the operational section of this specification is not implied. Exposure to absolute maximum rating conditions for extended periods may affect device reliability.

Table 3. Package Characteristics

Package Type	θ_{JA}	θ_{JC}	Device Weight
8-Lead CLCC	120°C/W	20°C/W	<1.0 gram

ESD CAUTION

ESD (electrostatic discharge) sensitive device. Electrostatic charges as high as 4000 V readily accumulate on the human body and test equipment and can discharge without detection. Although this product features proprietary ESD protection circuitry, permanent damage may occur on devices subjected to high energy electrostatic discharges. Therefore, proper ESD precautions are recommended to avoid performance degradation or loss of functionality.

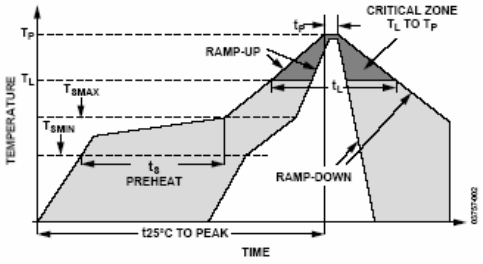

Profile Feature	Condition	
	Sn63/Pb37	Pb-Free
Average Ramp Rate (T_L to T_P)	3°C/second max	
Preheat		
• Minimum Temperature (T_{SMIN})	100°C	150°C
• Maximum Temperature (T_{SMAX})	150°C	200°C
• Time (T_{SMIN} to T_{SMAX}) (t_S)	60 to 120 seconds	60 to 150 seconds
T_{SMAX} to T_L		
• Ramp-Up Rate	3°C/second	
Time Maintained above Liquidous (T_L)		
• Liquidous Temperature (T_L)	183°C	217°C
• Time (t_L)	60 to 150 seconds	60 to 150 seconds
Peak Temperature (T_P)	240°C + 0°C/−5°C	260°C + 0°C/−5°C
Time Within 5°C of Actual Peak Temperature (t_P)	10 to 30 seconds	20 to 40 seconds
Ramp-Down Rate	6°C/second max	
Time 25°C to Peak Temperature	6 minutes max	8 minutes max

Figure 2. Recommended Soldering Profile

PIN CONFIGURATIONS AND FUNCTION DESCRIPTIONS

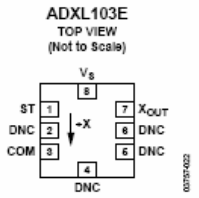

Figure 3. ADXL103 Pin Configuration

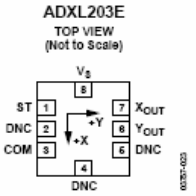

Figure 4. ADXL203 Pin Configuration

Table 4. ADXL103 Pin Function Descriptions

Pin No.	Mnemonic	Description
1	ST	Self Test
2	DNC	Do Not Connect
3	COM	Common
4	DNC	Do Not Connect
5	DNC	Do Not Connect
6	DNC	Do Not Connect
7	X_{OUT}	X Channel Output
8	V_S	3 V to 6 V

Table 5. ADXL203 Pin Function Descriptions

Pin No.	Mnemonic	Description
1	ST	Self Test
2	DNC	Do Not Connect
3	COM	Common
4	DNC	Do Not Connect
5	DNC	Do Not Connect
6	Y_{OUT}	Y Channel Output
7	X_{OUT}	X Channel Output
8	V_S	3 V to 6 V

ANALOG DEVICES

Dual Axis Accelerometer Evaluation Board

ADXL203EB

GENERAL DESCRIPTION

The ADXL203EB is a simple evaluation board that allows quick evaluation of the performance of the ADXL203 dual axis ±1.7 *g* accelerometer. The ADXL203EB has a 5-pin 0.1 inch spaced header for access to all power and signal lines that the user can attach to a prototyping board (breadboard) or wire using a standard plug. Four holes are provided for mechanical attachment of the ADXL203EB to the application.

The ADXL203EB is 20 mm × 20 mm, with mounting holes set 15 mm × 15 mm at the corners of the PCB.

CIRCUIT DESCRIPTION

The schematic and parts list of the ADXL203EB are shown in Figure 1. Analog bandwidth can be set by changing capacitors C2 and C3. See the ADXL203 data sheet for a complete description of the operation of the accelerometer.

The part layout of the ADXL203EB is shown in Figure 2. The ADXL203EB has two factory-installed 100 nF capacitors (C2 and C3) at X_{OUT} and Y_{OUT} to reduce the bandwidth to 50 Hz. Many applications require a different bandwidth, in which case the user can change C2 and C3, as appropriate.

SPECIAL NOTES ON HANDLING

The ADXL203EB is not reverse polarity protected. Reversing the +V supply and ground pins can cause damage to the ADXL203.

Dropping the ADXL203EB on a hard surface can generate several thousand *g* of acceleration and might exceed the data sheet absolute maximum limits. See the ADXL203 data sheet for more information.

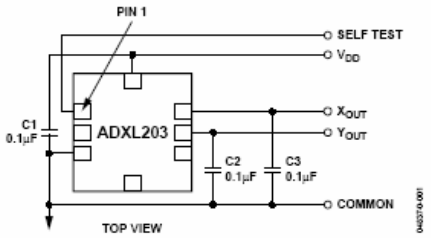

Figure 1. ADXL203EB Schematic

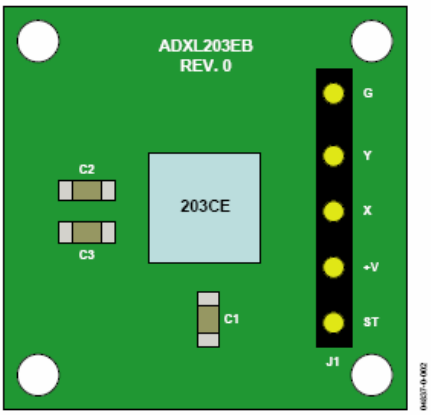

Figure 2. ADXL203EB Physical Layout

ORDERING GUIDE

Model	Package Description
ADXL203EB	Evaluation Board